Al-Quds University

Deanship of Graduate Studies

Mechanistic of the Interaction between Bovine Serum Albumin and Gold Nanoparticles

Ashraf Kamel Mohamad Jawade

MS Thesis

Jerusalem – Palestine
1439/2017

Mechanistic of the Interaction between Bovine Serum Albumin and Gold Nanoparticles

Prepared by:
Ashraf Kamel Mohamad Jawade
BS.c Physics, Al - quds University, Palestine

Supervisor: **Professor Musa Abu-Teir**
Co-Supervisor: **Dr. Hussain Alsamamra**

A thesis submitted in partial fulfillment of requirement for the degree of Master of Science in Physics, Faculty of Science And Technology – Deanship of Graduate Studies, Alquds University.

1439/2017

Al-Quds University

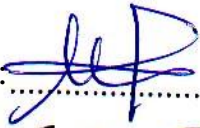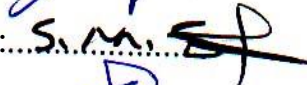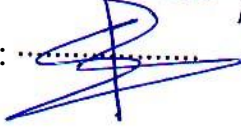**Deanship of Graduate Studies**

Department of Physics

Thesis Approval
Mechanistic of the Interaction between Bovine Serum Albumin and Gold Nanoparticles

Ashraf Kamel Jawade
Registration No: 2111099

Supervisor: Prof. Musa Abu-Teir
CO- Supervisor: Dr. Husain Alsamamra

Master thesis submitted and accepted, Date: 13 /1 / 2018

Names and signatures of the examining committee members

1. Head of the committee: Prof. Musa Abu-Teir   Signature:

2. Internal Examiner: Prof. Salman M Salman   Signature:

3. External Examiner: Prof. Mustafa Abu Safa   Signature:
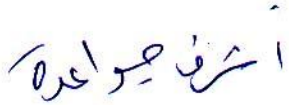
Jerusalem – Palestine
1439/2017

Dedication

I dedicate this thesis to my wonderful family members who have supported me throughout my life to achieve my goals. To my parents for their unconditional love, guidance, and support. To my brothers and sisters. A special thank you to my wife for her support and encouragement support through life. I love you all.

Ashraf Kamel Jawade

Declaration

I hereby declare that this thesis is based on the results found by myself. Materials of works found by other researchers are mentioned by references. This thesis, neither in whole or in part, has been previously submitted for any degree.

Sign:

Name: Ashraf Kamel Mohamad Jawade

Date: 13/1/2018

Acknowledgements

At first and at last, my Great commendation and Thanks to Allah, who gave me the ability to accomplish this work, and created such nice supporting people.

Many thanks to my advisors Professors Musa Abu-Teir and Husain Alsamamra, who helped me to work in Biophysics and for their encouragement during my work. I want to thank Professor Saker Darwish for his help. I would also like to thank Al-Quds University nano-technology laboratory staff for their help and efforts.

Thanks, respect, and appreciation to Professor Salman M. Salman for his critical and comprehensive review that helped reach this quality level in writing or content.

Ashraf kamel Jawade

Abstract

The interaction of gold nanoparticles (AuNPs) of two sizes (40 and 60 nm) with Bovine Serum Albumin (BSA) was investigated using UV visible absorption spectroscopy (UV-VIS), Fluorescence Spectroscopy, and Fourier Transform Infrared Spectroscopy (FTIR).We have tested 5 BSA-Gold mixed ratios for the two sizes of 40 and 60 nm and applied the three spectroscopic methods in addition to testing BSA samples free of gold for reference. A total of 33 samples were used and all samples preparations were done at room temperatures.

We have measured the BSA-Gold binding constants for the two Gold sizes using at different concentrations. The UV-VIS measurement values are ($0.888 \times 10^4 M^{-1}$ and $1.16 \times 10^4 M^{-1}$). The fluorescence spectroscopy measurements values for the constants came as (0.92×10^4 M^{-1}) and ($1.3 \times 10^4 M^{-1}$) for the two gold sizes respectively. In addition, the Stern-Volmer constants were calculated for the same samples and the values came as (2.17×10^2 L mol^{-1}) and (4.5×10^2 L mol^{-1}). The variations in these constant between the 40nm and the 60nm indicates the interaction dependence on the particle size which can affect the bonding configurations. The conclusion was also observed in the FTIR data.

The fluorescence data reveals a decrease in Bovine Serum Albumin (BSA)emission intensity with the increase of gold particles ratio in BSA-Gold mixtures. This decrease in intensity indicates the Gold has a strong ability to quench the BSA intrinsic fluorescence through static quenching mechanism.

With FTIR data peaks positions in the amide I, amide II and amid III regions were measured and the concentration variation effects have been investigated. The peaks positions for all three amid bands showed a shift toward high wave numbers or energy of the peaks positions, while for the last two peaks of the amid III band the behavior was the opposite.

The absorption bands intensities showed correlation and dependence on the ligand concentration. The intensity generally decreased with the increase of the gold ratio in the mixed complexes. Further work to investigate these correlations using wide range of gold particles size or using other proteins may yield more information about these interactions.

Table of Contents

List of Tables

List of Figures

List of Symbols

Symbol	Description
[L]	The quencher concentration.
A	Constant for a particular molecule.
A	The recorded absorption at different Testosterone concentrations (L).
A0	The initial absorption of protein at 280 nm in the absence of ligand
A∞	The final absorption of the ligated protein
B	The path length
C	Speed of light
Deq	The dissociation energy.
E total	Total energy
Eele	Electronic energy
Eo (v)	The maximum amplitude of the beam at z=0
Erot	Rotational energy
Ev	The potential energy for harmonic oscillator approximation
Evib	Vibrational energy
F	Fluorescence intensity with quencher
Ƒ	The spring or force constant
F0	Fluorescence intensity without quencher
Fx	Restoring force acts on the spheres
H	Planck's constant
hυEM	Energy of photon emitted

hυEX	The excitation photon energy
I(z1, z2, v) dv	The intensity after recombination of the beams for the fixed spectral range dv
I0	The radiant power incident on the sample
K	Binding constant
Ksv	The Stern-Volmer quenching constant
mA, mB	Mass of particles A,B
S(v)	The spectrum
S0	The ground singlet electronic state
S1 and S2	The successively higher energy excited singlet electronic states
T	The kinetic energy of the oscillating motion
T1	The lowest energy triplet state
V	The potential energy
V	Circular frequency in wave-numbers
V	Vibrational level
we	Oscillating frequency
ŵe	Oscillation frequency in wave number
Xe	The an-harmonicity constant
Δ	Un-saturation site
Δx	Displacement of the spheres along the x-axis from equilibrium position
E	molar extinction coefficient
λ	Wavelength
μ	The reduced mass
N	Frequency
T	The unquenched lifetime
kq	The bimolecular quenching constant
ω	Circular frequency of the harmonic vibration

List of Abbreviations

Abbreviation	Abbreviation representation
BSA	Bovine Serum Albumin
C	Concentration
Diff	Difference
EM	Electromagnetic
Eq.	Equation
FS	Fluorescence Spectroscopy
FSD	Fourier self deconvolution
FT-IR	Fourier Transform Infrared
Gold xxx nm-BSA	Gold nanoparticles size xxx nm with BSA complex
IR	Infra-red
KDa	Kilo Dalton
LED's	Light emitting diodes
MCT	Mercury Cadmium Telluride
Mid-IR	Middle infrared
MIR	Magnetic Imaging Resonance
MRI	Magnetic resonance image
Nm	Nanometer
OPUS	Optical User Software
Or BSA-gold xxx nm	Gold nanoparticles size xxx nm with BSA complex
PET	Positron Emission Tomography
pH	Power of hydrogen
T	Transmittance
UV-VIS	Ultra Violet Visible Absorption Spectrophotometer
α-helix	alpha helix
β-sheets	Beta sheets

Chapter One: Introduction

Infrared spectroscopy is a technique based on the vibrations of the atoms of a molecule. An infrared spectrum is commonly obtained by passing infrared radiation through a sample and determining what fraction of the incident radiation is absorbed at a particular energy. The energy at which any peak in an absorption spectrum appears corresponds to the frequency of a vibration of a part of a sample molecule **[Banwell, C. N. 1972]**.

The main goals of molecular spectroscopy are firstly to understand the light interaction in with matter and its quantitative use to understand sample, which is our topic of concern in this research. Secondly spectroscopy methodology is used to solve scientific problem, for example by keeping the idea of "what does the light do in the sample" in mind. **[Banwell, C. N. 1972]**.

Infrared spectroscopy is an absorption method in the wavelength region of 1 to 100 μm in that extends the region of the visible light to longer wavelengths and smaller frequencies/energies. The energy of infrared light is not sufficient to induce transitions of valence electrons. Instead, infrared radiation excites vibrational and rotational motions in molecules. Except for the differences in the energy transfer from the radiation to the molecule, the principles of IR spectroscopy are the same as those of VIS/UV spectroscopy or other spectroscopic techniques [**Wilson, E. 1995**].

The absorption of infrared light is again characterized by the Bouger-Lambert-Beer Law [Schulman, S.G. 1977], [**Hollas, M.J. 2004**]. However, infrared spectra are usually presented by a plot of the percentage of transmission vs the wavenumber in cm^{-1} (as opposed to a plot of absorbance vs. the wavelength in nm in UV/VIS spectroscopy). A typical IR spectrum is therefore recorded from about 4 000 to 10 000 cm^{-1} (upper limit) to about 100-800 cm^{-1} (lower limit).

Atoms can move relative to each other causing the bond to vary in length, this causes bond stretching, or one atom can move out of plane relative to the other, causing bond bending. Resonance frequencies for linear molecules 3N-5 while they are 3N-6 for nonlinear molecule some of which will interact with incident infrared radiation [**Gordon G. Allison 2011**].

Serum albumin, often referred to as blood albumin, is a type of globular protein found in vertebrates blood. Human serum albumin is encoded by the ALB gene. Other mammalian forms, such as bovine serum, are chemically similar [**Hawkins JW1982**].

Serum albumin produced by the liver occurs dissolved in blood plasma, and it is the most abundant blood protein in mammals. It is essential for maintaining the oncotic pressure needed for proper distribution of body fluids between blood vessels and body tissues; without it, the high pressure in the blood vessels would force more fluids into the tissues.
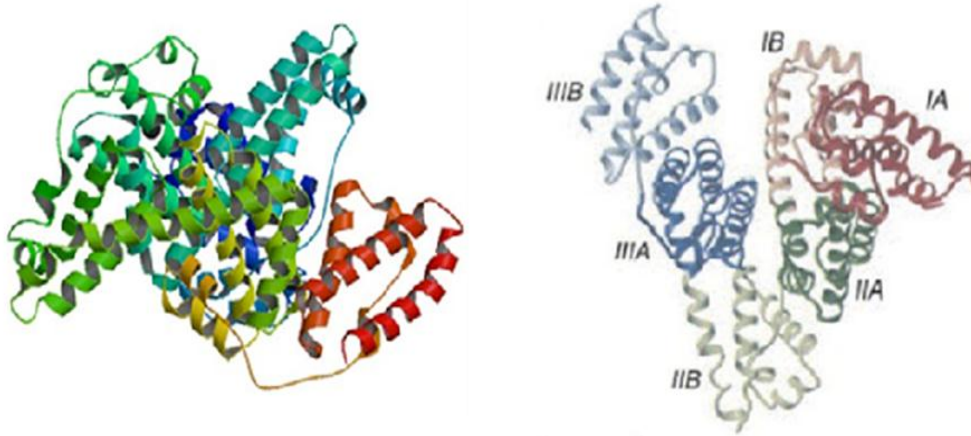
Figure 1.1: The heart-shaped serum albumin molecule consists of three homologous α-helical domains (I, II, III). Each domain contains two subdomains (A and B) that share common structural motifs .

It also acts as a plasma carrier by non-specifically binding several hydrophobic steroid hormones and as a transport protein for hemin and fatty acids. Too much or too little circulating serum albumin may be harmful. Albumin in urine usually denotes the presence of kidney disease. Occasionally it appears in the urine of normal persons following long standing (postural albuminuria) [**Dugaiczyk A . 1983**].

Gold nanoparticles: have been utilized for centuries by artists due to their vibrant colors produced by their interaction with visible light. Their unique optoelectronic properties have been researched and utilized in high technology applications such as organic photovoltaics, sensory probes, therapeutic agents, drug delivery in biological and medical applications, electronic conductors and catalysis. The optical and electronic properties of gold nanoparticles are tunable by changing the size, shape, surface chemistry, or aggregation state[**Ali, M. E 2012**].
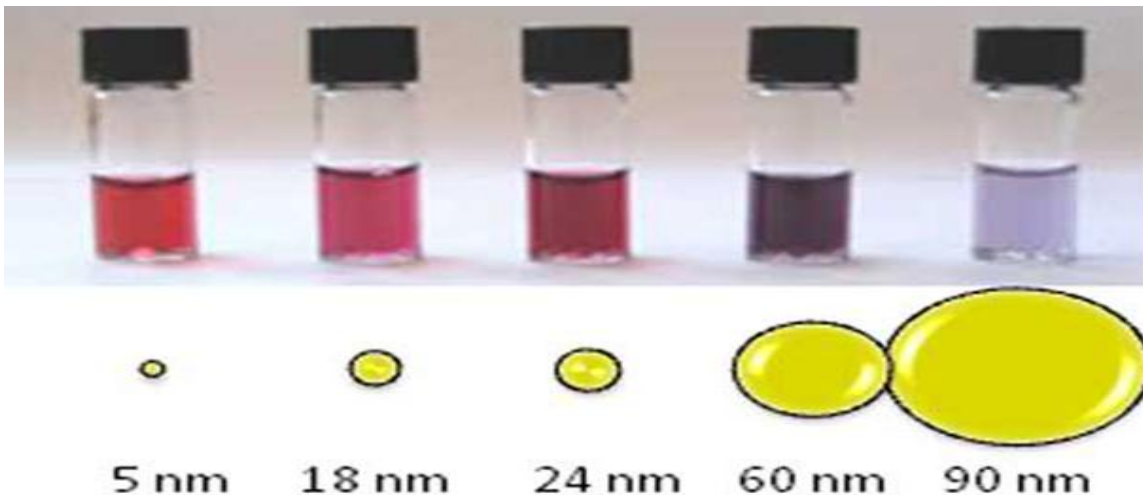
Figure 1.2: Suspensions of gold nanoparticles of various sizes. The size difference causes the difference in colors.

This thesis includes five chapters; chapter 2 will discuss the theoretical aspects and experimental methods important for this study. Chapter 3describes the experimental procedures, and instruments used. In chapter 4 the results obtained are presented and discussed. Final chapter 5 summarizes the conclusions and future work.

One of the studies is titled Spectroscopic Studies on the Mechanism of Interaction of Vitamin B12 with Bovine serum albumin**[Maruthamuthu, M. 1987]**.The mechanism of interaction of cyanocobalamin (CB) with BSA has been investigated by spectrofluorometric and circular dichroism methods. The association constant for the CB-BSA system showed that the interaction is non-covalent in nature.

Binding studies in the presence of a hydrophobic probe, 8-anilino-1- naphthalene sulfonic acid, sodium salt (ANS) showed that there is hydrophobic interaction between CB and ANS and they do not share common sites in BSA. Stern-Volmer analysis of fluorescence quenching data showed that the fraction of fluorophore (protein) accessible to the quencher (CB) was close to unity indicating that both tryptophan residues of BSA are involved in drug-protein interaction. The rate constant for quenching, greater than 10^{10} M^{-1} s^{-1}, indicated that the drug binding site is in close proximity to tryptophan residue of BSA**[Darwish, S. M. 2012].**

Thermodynamic parameters obtained from data at different temperatures showed that the binding of CB to BSA involves hydrophobic bonds predominantly. Significant increase in concentration of free drug was observed for CB in presence of paracetamol. Circular dichroism studies revealed the change in helicity of BSA due to binding of CB to BSA[C-Qui Jiang 2002].

In another study entitled Spectroscopic Approach of Protein- Androgen Complexes: Study of Testosterone Interactions with Human Serum Albumin. It was relatively high binding affinity between Testosterone and Human Serum Albumin[E.K.Oyakawa2004].

In this work we have studied the interaction between gold nanoparticles of two sizes (40 &60 nm) with BSA as carrier using spectroscopic techniques. The binding constants and the quenching values were obtained using UV-visible whereas the spectrums of the interaction was obtained using FT-IR.

Chapter Two: Background

The chapter reviews the theory of molecular energy spectra, the various spectroscopy methods and principles and coverage of certain proteins and the BSA interactions with gold nano particles.

2.1 Molecular energy spectra

This section reviews vibrational spectra and the associated vibrational and rotational energy modes with coverage for the diatomic and poly atomic molecules.

2.1.1 Electromagnetic spectrum and absorption of light
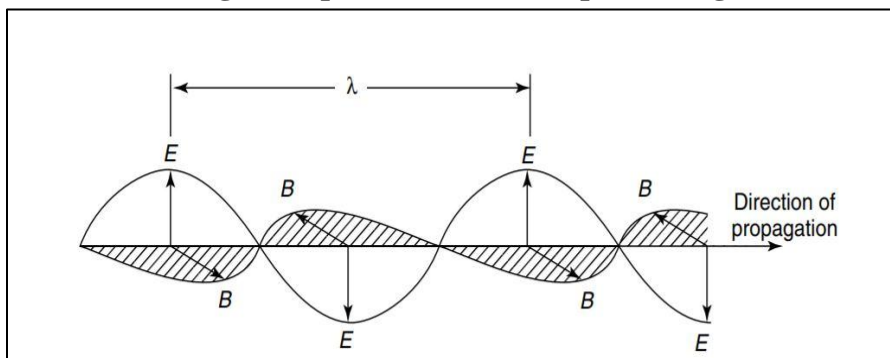
Figure 2.1: Representation of an electromagnetic wave [Stuart, B. 2004]

Electromagnetic radiation consists of electric and magnetic fields, propagating at the speed of lights as sine waves oscillating is phase in single planes at right angles to each other [Stuart, B. 2004]. The wave can be considered as plane- polarized radiation [Hollas, M.J. 2004]. The directions of the electric and magnetic field vectors represented are shown in Figure.2.2 [Stuart, B. 200], [Hollas, M.J. 2004)].
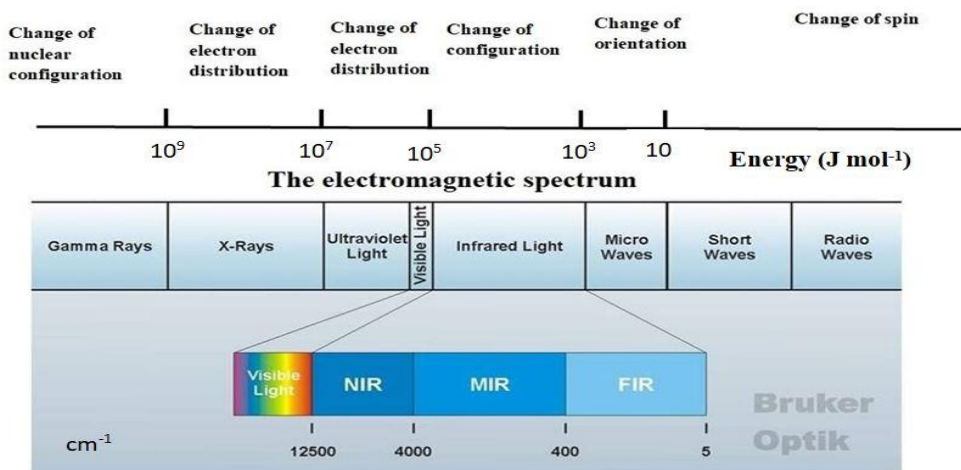
Figure 2.2: Regions of the Electromagnetic spectrum [OPUS Bruker 2004],[Stuart,B. 2004]

The electromagnetic spectrum can be divided into different regions as shown in Figure 2.3 according to the photons energies and hence their chemical and physical effects they produce when interacting with matter[Stuart, B. 2004], [Derrick. M. R, 1999].

The amplitude measures the intensity, the frequency v measures the energy, and the wavelength λ measures the uncertainty in the locating this energy. The wavenumber $\tilde{v}$ can be expressed as $1/\lambda$ in units of in cm^{-1}. It is useful to study the absorption spectra for various regions and from it one can measure certain properties of the materials studied.
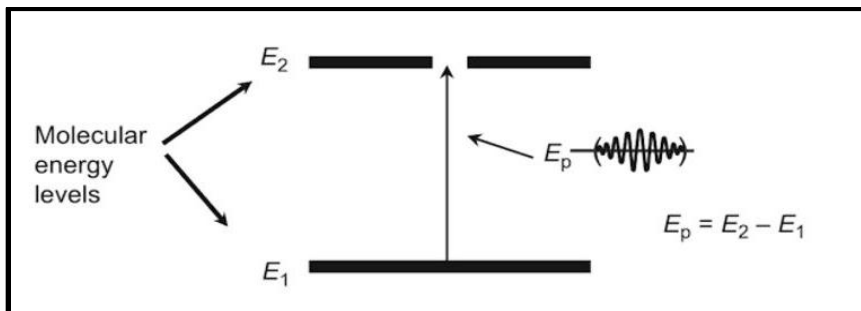
Figure 2.3: Absorption of electromagnetic radiation [Ball, D.W. 2001].

Sourcesemit radiation in discrete units of energy depending on it spectra structures. The photon energy E$_p$ is related to frequency v by $E_p = hv,$ h is Planck's constant.

Photons may be absorbed, scattered or transmitted through matter with large or small loss of energy based on the photon energy and the material spectral structure and generally that defines the interaction cross section between the photons and that matter.

For molecules the energy structure is described in the rotational and vibrational bands. They are a result of the local motion of molecules and that changes the potential and the energy structure. If the energy of an incident photon equals some energy gap between the ground and some excited state, the photon may be absorbed and the molecule is excited to the higher energy state with a change of energy equals to E_p as shown in Figure 2.4 [Ball, D.W. 2001].The energy possessed by a molecule from electromagnetic wave is given by:

$$E_{total}=E_{elec}+ E_{vib} + E_{rot} + E_{trans} \qquad (1)$$

The translational energy (E$_{trans}$) describes the displacement of molecules from its equilibrium position. The rotational energy (E$_{rot}$) is the result of the absorption within the microwave region, where the molecule rotates around its center of mass. The vibrational energy corresponds to the absorption by a molecule where the atoms vibrate about the mean center of their chemical bonds (they change their relative repulsive and attraction forces between the atoms and their constituents) [Sharma, B.K. 2007].

2.1.2 Vibrational and rotational energy modes

Normal modes and degrees of freedom

In a molecule, the atoms are constrained by molecular bonds to move together in certain ways, called degrees of freedom [Derrick M. R. 1999]. Considering a molecule contains N atoms their position can be defined by specifying three coordinates for each yielding 3N degrees of freedom for the molecule. For a molecule, three degrees go for translational motion, and another three in a nonlinear molecule go to rotational motion. For a linear molecule only two are due to rotational motion.

Table 2.1: Degrees of freedom for polyatomic molecules [Stuart, B. 2004].

Type of degrees of freedom	Linear	Non linear
Translational	3	3
Rotational	2	3
Vibrational	3N-5	3N-6
Total	3N	3N

Normal modes of vibration occur when all atoms undergo harmonic motion in phase and with the same frequency but with different amplitudes. For linear molecules, there are 3N-5 vibrational mods, where for Non-linear molecules there are 3N-6 vibrational mods as shown in Table 2.1[Nikolić, G. S. 2011],[Banwell, C. N. 1972].

4 Group frequencies

Within the molecule there are two or more bonds close together with similar energies. These bonds form the so called functional groups (carbonyl or amide groups).

Table 2.2: Group vibration wavenumbers for some-stretching bending vibrations [Hollas, M.J. 2004].

Bond-stretching		Bond-stretching		Angle-bending	
Group	ω/cm^{-1}	Group	ω/cm^{-1}	Group	ω/cm^{-1}
≡C—H	3300	—C≡N	2100	≡C—H	700
=C<H	3020	>C—F	1100	=C<H,H	1100
except: O=C<H	2800	>C—Cl	650	—C<H,H	1000
>C—H	2960	>C—Br	560	>C<H,H	1450
—C≡C—	2050	>CI—I	500	C≡C—C	300
>C=C<	1650	—O—H	3600[a]		
>C—C<	900	>N—H	3350		
≡Si—Si<	430	>P=O	1295		
>C=O	1700	>S=O	1310		

When the selection rules for IR absorption are met, these groups absorb IR photons increasing the amplitude of the harmonic oscillation of the group's atoms compared to the other atoms in the molecule [Derrick, M. R. 1999]. A group vibration wavenumbers for some-stretching and bending vibrations are listed in Table.2.2 [Hollas, M. J. 2004].

This group absorption occurs independent of the rest of the molecule atoms. The absorption group frequency is characteristic for that group [Derrick. M. R. 1999].

2.1.3 Vibrational energy for a diatomic molecule

Molecular bonds can vibrate in different modes of vibration; the stretching vibration is when the bond length is changed. All other modes are called deformation modes, such as the bending vibration where the bond **angle** is changed as in Figure 2.4 [Stuart. B, 1997]; [Schrader, 1995].For a diatomic molecule there is only one vibrational normal mode which is the stretching vibration [Stuart, B 2004]. The polyatomic molecules, number of stretching vibrations is equal to the number of valence bonds and the rest are bending vibrations [Sathyanarayana, D.M. 1983].
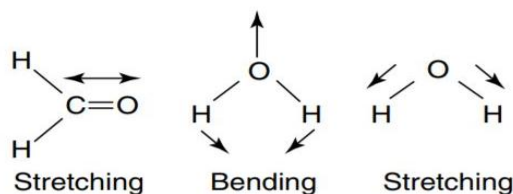
Figure 2.4: Stretching and bending vibrations [Stuart. B. 1997]

Molecular bonds may stretch in-phase (symmetrical stretching) or out-of-phase (asymmetrical stretching) as shown Figure.2.5 [Stuart, B. 1997]. Symmetrical molecules which are IR- active vibrate at fewer frequencies than the asymmetrical molecules [Stuart. B, 2004].
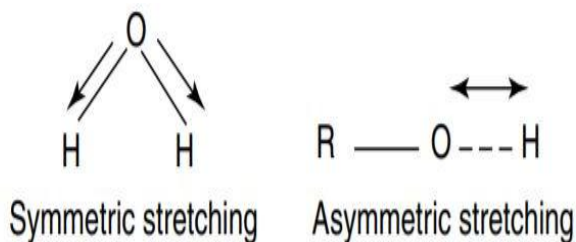
Figure 2.5: Symmetric and Asymmetric stretching vibrations [Stuart, B. 1997].

The displacement of the atom from its equilibrium position changes periodically with time at the same frequency but with different amplitudes. Figure 2.4 shows the atomic displacement vs. time [Williams, D. 1976].

Classical calculations Figure 2.6 show a scheme model of the atoms bonds in a molecule as balls of masses m_1 and m_2 connected by a massless string.
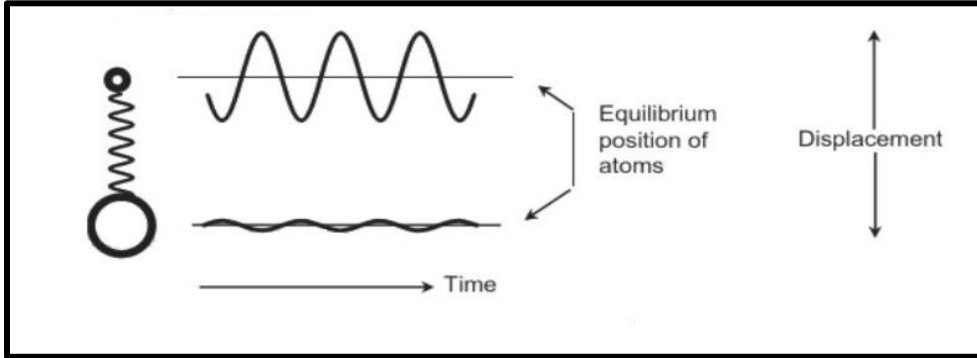
Figure 2.6: The ball and spring model for a diatomic molecule [Williams, D. 1976].

In the harmonic oscillator model the restoring force, **obeys**Hooke's law,with x the displacement of the atom from the equilibrium position the force is given by

$$\mathbf{F} = -k\,x \qquad (2)$$

Where k is the force constant of the spring, and measures the strength of the bond between the two atoms. Molecular bonds vibrate with a specific frequency that is called the vibrational frequency (v).

$$v = \frac{1}{2\pi c}\sqrt{\frac{k}{\mu}} \qquad (3)$$

Where v is the fundamental vibration frequency, c is the speed of light and μ is the reduced mass [Sharma, B.K. 2007].

$$\mu = \frac{m_1 m_2}{m_1 + m_2} \qquad (4)$$

And the vibrational energy is:

$$E = \frac{1}{2}k(r - r_{eq})^2 \qquad (5)$$

Where is the internuclear distance and r_{eq} is the equilibrium distance.

Quantum calculations: The Schrodinger equation for one-dimensional harmonic oscillator is given by:

$$\frac{d^2\Psi_v}{dx^2} + \left(\frac{2\mu E_v}{h^2} - \frac{\mu k x^2}{h^2}\right)\Psi_v = 0 \tag{6}$$

The vibrational energy $E_{nv} = hv(n + 1/2)$ $(n = 0, 1, 2,$ is the vibrational quantum number$)$
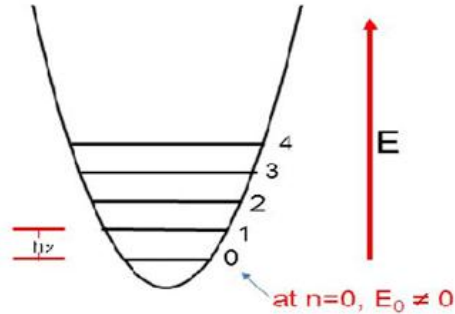
Figure 2.7: The allowed vibrational energy levels for harmonic oscillator [OPUS Bruker 2004]

The possible transitions are those which satisy the selection rule $\Delta n = \pm 1$. The allowed vibrational energy levels for diatomic molecules are shown in Figure.2.8 [Hollas, M.J. 2004], [OPUS Bruker 2004], [Gupta 2001].

2.1.4 Vibrational energy for polyatomic molecules

For polyatomic moleule there are 3N-5 and 3N-6 vibrational modes for linear and Non-linear moleules respectively as will be discussed in (sec. 2.3.2). The vibrational energy for each normal mode is given by:

$$E_k = hv\left(v_k + \frac{1}{2}\right) \tag{7}$$

Where V_k is the vibrational quantum number of the Kth normal mode. The total energy for Non-Linear molecule is the sum of the energies associated with each normal mode .

$$E_{vib} = \sum_{k=1}^{3N-6}\left(v_k + \frac{1}{2}\right)hv_k \tag{8}$$

The lowest vibrational energy (i.e. when $V_k = 0$), which is the energy of the ground vibrational level and called the zero-point energy, is given by:

$$E_. = \frac{1}{2}\sum_{K=1}^{3N-6}hv_k \tag{9}$$

When the anharmonicity is applied, then the vibrational energy for the polyatomic moleule is given by:

9

$$E_{vib} = \sum_{K=1}^{3N-6}(v_k + \frac{1}{2}) + \sum_{i=1}^{3N-6} \sum_{k\geq i} hx_{ik(v_{i+\frac{1}{2}})}(v_k + \frac{1}{2}) + hG \tag{10}$$

Where G is a constant that arises partly from deviation from harmonic motion and partly from vibration-rotation interaction. It is usually omitted since it is very small, and it has been added to emphasize that the vibrational frequencies correspond to the equilibrium positions [Banwell, C. N. 1972].

2.1.5 Anharmonic oscillations

Real molecules don't obey the harmonic oscillations due to the following reasons; the first reason is that when two atoms approach each other, there must be a repulsive force between them, thus the vibrational energy will increase very rapidly.

The second reason is that when the two atoms go far away from each other, the bond between them will be broken; at this point, the vibrational energy equals the dissociation vibrational energy for diatomic molecule must be modified to apply they anharmonicity. The function which represents this is the Function[Morse, P. M. 1929]:

$$E = D_{eq}\left[1 - \exp\left\{a(r_{eq} - r)\right\}\right]^2 \tag{11}$$

Where D_{eq} is the dissociation energy, which is constant for a particular molecule.

When the Morse energy function inserted to the Schrodinger equation instead of (Eq. 5), then the vibrational energy will be :

$$\varepsilon_v = (v + \frac{1}{2})\varpi_e - (v + \frac{1}{2})^2 \varpi_e x_e \tag{12}$$

Where ϖ_e, is the oscillation frequency expressed in wavenumbers and x_e is the anharmonicity constant. The selection rules are: $\Delta v = \pm 1, \pm 2, \pm 3$. which are the same of that for the harmonic oscillator in addition to the possibility of larger jumps. The allowed vibrational energy levels for anharmonic oscillator are shown in (Fig.2.8).

The transition from v = 0 to v = 1 is called the fundamental vibration, from v = 0 to v = 2 is called the first overtones and from v = 0 to v = 3 is called the second overtone. Where the transitions for $\Delta v = \pm 2, \pm 3$. are called the hot transitions, and these absorptions are weaker than the other transitions [Banwell, 1972], [OPUS Bruker 2004].
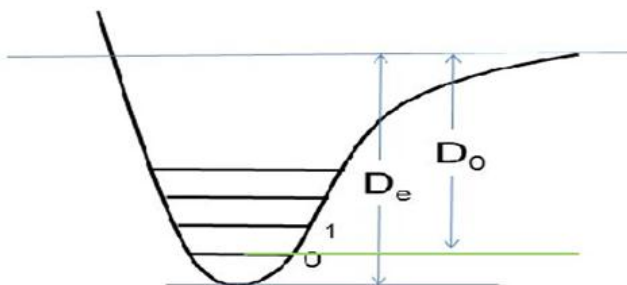
Fig2.8: Potential energy curve for anharmonic oscillator [Bernath 2005].

2.2 Spectroscopy methods and instruments

This section covers absorption of infrared light, the IR spectrometers and advantages of FTIR spectrometers and the interpretation of IR-spectra. In addition we cover the UV-VIS spectroscopy we used to measure the binding constant between the ASA and the vitamin.

2.2.1 Ultraviolet-Visible (UV-VIS) spectrophotometer

A NanoDrop (ND-1000) spectrophotometer which is shown in Figure 2.9 was used to give the absorption spectrum in the range of (220-750) nm. It has two fiber optic cables; the receiving and the source fibers with a gap between their ends.

The light source is a pulsed xenon flash lamp, and a spectrometer utilizing a linear CCD array is used to analyze the light after passing through the sample. Special software run from a PC controlled the instrument, and the data is logged in an archive file on the PC [NanoDrop 1000 Spectrophotometer V3.7],[User's Manual. 2008].

Figure 2.9:NanoDrop (ND-1000) spectrophotometer.

2.2.2 Fluorescence Spectrophotometer

When continuous radiation passes through a transparent material, a portion of the radiation may be absorbed. In the case of UV-VIS spectrophotometer, the transitions that result in the absorption of electromagnetic radiation in this region of the spectrum are transitions between

11

electronic energy levels. As a molecule absorbs energy, an electron is promoted from an occupied orbital to an unoccupied orbital of greater potential energy.
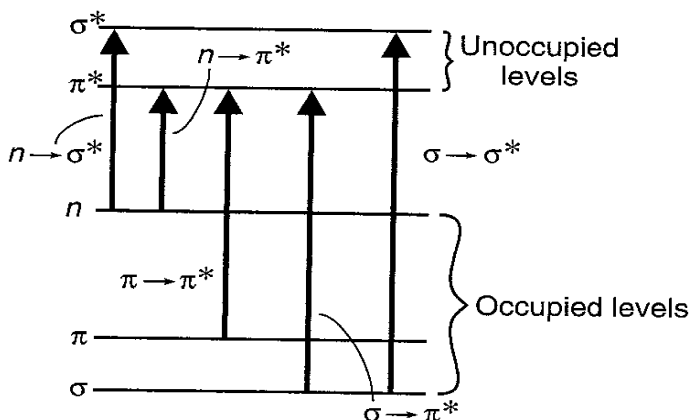
Figure 2.10: Electronic energy transitions

For most molecules, the lowest –energy occupied molecular orbitals are the σ orbitals, which correspond to σ bonds. The π orbitals lie at some higher energy levels, and orbitals that hold unshared pairs, the nonbonding (n) orbitals , lie at even higher energies .The unoccupied, or anti bonding orbitals (π*and σ*) [Pavia 2009].In all compounds, the electrons may undergo several possible transitions of different energies figure (2.10) illustrates these transitions .

Fluorescence spectrophotometry is a class of techniques that assay the state of a biological system by studying its interactions with fluorescent probe molecules [Dong, C. Y 2002]. Luminescence is emission of light by a substance not resulting from heat; it is thus a form of cold body radiation. Luminescence is formally divided into two categories fluorescence and phosphorescence depending on the nature of the excited states [Soukpo´e-Kossi2007]. Fluorescence and phosphorescence are photon emission processes that occur during molecular relaxation from electronic excited states.

Fluorescence is that process in which the emission of light by a substance that has absorbed light or other electromagnetic radiation [Johnson. L 2010]. A fluorophore is a molecule that is capable of fluorescing. In its ground state, the fluorophore molecule is in a relatively low energy, stable configuration, and it does not fluoresce. Fluorophore is unstable at high energy configurations, so it eventually adopts the lowest-energy excited state, which is semi-stable. The process responsible for the fluorescence of fluorescent probes and other fluorophores is illustrated by the simple electronic-state diagram (Jablonski diagram) shown in Figure 2.11.
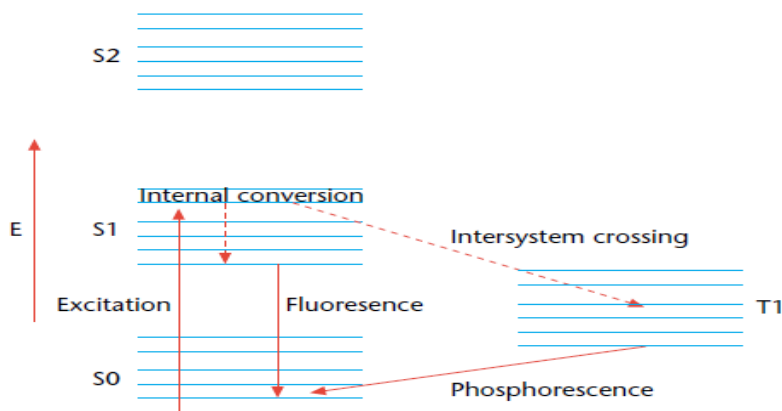
Figure 2.11: The Jablonski diagram of fluorophore excitation [Dong, C.Y 2002].

Where E denotes the energy scale; S0 is the ground singlet electronic state, S1 and S2 are the successively higher energy excited singlet electronic states. T1 is the lowest energy triplet state [Dong, C.Y 2002]. The fluorescence lifetime and quantum yield are the most important characteristics of a fluorophore. Quantum yield is the number of emitted photons relative to the number of absorbed photons. The lifetime is determined by the time available for the fluorophore to interact with or diffuse in its environment, and hence the information available from its emission [Lakowicz, J.R. 2006].

Fluorophores are divided into two main classes. First intrinsic fluorophores are those that occur naturally, such as aromatic amino acids. Secondly extrinsic fluorophore are added to the sample to provide fluorescence when none exists, or to change the spectral properties of the sample [Lakowicz, J.R. 2006]. After the excitation occurs, the excited state exists for a finite time (typically 1-10 nanoseconds). During this time; the fluorophore undergoes conformational changes and is also subject to a multitude of possible interactions with its molecular environment.

These processes have two important consequences. First, the energy of S2 is partially dissipated, yielding a relaxed singlet excited state (S1) from which fluorescence emission originates. Second, not all the molecules initially excited by absorption return to the ground state (S0) by fluorescence emission.

At **Fluorescence Emission stage** a photon of energy hυEM is emitted, returning the fluorophore to its ground state S0. Due to energy dissipation during the excited-state lifetime, the energy of this photon is lower, and therefore of longer wavelength, than the excitation photon hυEX. The difference in energy or wavelength represented by hυEX – hυEM) is called the Stokes shift [Johnson. L 2010].

Fluorescence spectroscopy can be applied to a wide range of problems in the chemical and biological sciences. The measurements can provide information on a wide range of molecular

processes, including the interactions of solvent molecules with fluorophores, conformational changes, and binding interactions [Lakowicz, J. R. 2006].

2.2.3 FTIR spectroscopy

IR spectroscopy can be used to determine the chemical functional groups, as they absorb characteristic IR spectra. Using various sampling accessories, IR spectrometers can study a wide range of sample types such as gases, liquids and solids. Moreover, IR spectroscopy is important for structural elucidation and compound identification [Shernan M. 2014]. We will review the absorption relations with the compounds structures and then introduce the various aspects of the absorption spectra, and finally we introduce the Furrier Transform IR instrument as it will be used in this work.

1. IR- absorption

IR absorption is the process where the molecules are excited by photons to a higher energy states. IR radiation does not have enough energy to induce principal electronic transitions as seen with UV and visible light. The energy is in the range of 8 to 40 KJ/mole. It can only excite the molecules vibrational and rotational states encompassing the stretching and bending vibrational frequencies of the bonds in many covalent molecules.
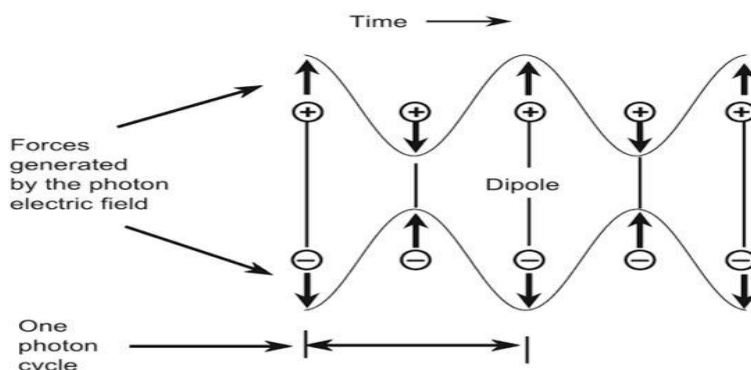
Figure 2.12: Changinf of the molecule's dipole moment with the oscillating photon's electric field [Raaman, N. 2006].

If the radiation frequency matches the vibrational frequency of the molecule then it will be absorbed, changing the amplitude of molecular vibration. In addition, absorption occurs only if the vibrations or rotations cause a net change in the molecule dipole moment as shown in Figure 2.12. [Sathyanarayana, D.M. 1983]. For example, homonuclear diatomic molecules such as H_2, N_2 and O_2 are IR- inactive, because they do not have dipole moments, while heteronuclear molecules such as HCI, NO and CO are IR-active because they have dipole moments [Raaman, N. 2006].

Infrared spectra show characteristic absorption peaks corresponding to vibrations of bonds between the molecule atoms. Therefore, infrared spectroscopy help identify the different materialsfrom the peaks locations. In addition the peak size reflects the elements amounts in the molecule providing a good quantitative measure of the molecular structure [Thermo Nicolet, 2001]. The Beer-Lambert equation relates the peak absorbance A to the concentration C, with (a) the absorptivity and b is the path length traveled by light through the sample [Workman. J .R. 1998].

$$A = abC \quad (13)$$

2. IR-spectra interpretations

When we plot the intensity of IR radiation absorbed or transmitted by the molecule versus the wavenumber we attain IR spectrum. The Y- axis may represent the absorbance or the transmittance of IR energy, where the x- axis represents the vibrational wavenumbers [Smith, B.C. 2011]. We can calculate the transmittance (T) from the absorbance (A) and vice versa according to the following relation:

$$A(\tilde{v}) = \log_{10} \frac{1}{T(\tilde{v})} \text{ and } T(\tilde{v}) = \frac{I(\tilde{v})}{I_{.}\tilde{v}} \quad (14)$$

Where I $(\tilde{v})$ is the intensity of the transmitted IR energy and $I_{.}(\tilde{v})$ is the intensity of irradiating IR energy [Griffiths, P.R2007]. IR spectrum provides us with quantitative or qualitative information.

Qualitative analysis

It provides us with qualitative information because each functional group in the molecule has its own peak of absorbance at specified frequency, so in our spectrum, if we have a peak at this frequency, it is evident that the molecule contain this functional group. For example, the peak around 300 cm^{-1} points to that this molecule contains C-H bond stretching [Smith, B.C. 2011].

**Quantitative analysis

It provides with quantitative information because we can calculate the concertation of matter we deal with using Beer's law, which relates the concentration to the absorbance at each component if the sample is a mixture as the following:

$$A_i(\tilde{v}) = a_i(\tilde{v})bc_i \quad (15)$$

Where $a_i(\tilde{v})$ is the linear absorption coefficient (cm^{-1}) at , $\tilde{v}$, b is the thickness of the sample and c_i is the concentration at component i.

For N-component mixtures where more than one component absorbs at $\tilde{v}$, the total absorbance is given by: [Griffiths, P.R2007].

$$A(\tilde{v}) = \sum_{i=1}^{N} \left[a_i(\tilde{v}) b c_i \right] \quad (16)$$

3. IR-Region

Infrared radiation spans a section of the electromagnetic spectrum having wavenumbers from roughly 13,000 to 10 cm-1, or wavelengths from 0.78 to about 1000 μm. It is bound by the red end of the visible region at high frequencies and the microwave region at low frequencies [Shernan, M. 2014]. IR spectroscopy people do not usually use the wavelength to plot their spectra but rather its inverse, wavenumber. Thus, wavenumbers are directly proportional to frequency, as well as the energy of the IR absorption. [Uversky V. N. 2007], [Shernan, M. 2014]. The IR region is commonly divided into three smaller areas: near IR, mid IR and far IR. Mid-IR between 400 and 40 cm-1 is the most frequently used region and it is what we have used in this study. The rough limits for each IR region are shown in the figure 2.13.
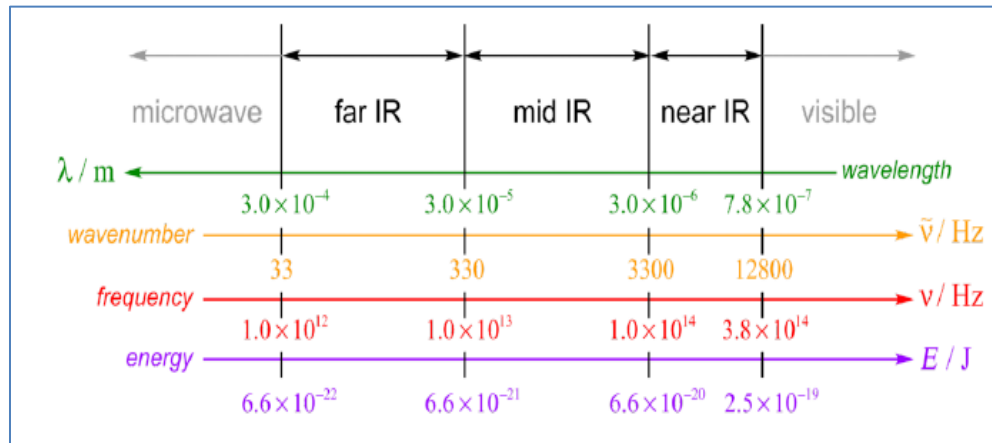
Figure 2.13: Regions of IR spectrum (benjamin-mills.com).

4. IR spectrum presentation

IR absorption information is generally presented in the form of a spectrum with wavelength or wave-number as the x-axis and absorption intensity or percent transmittance as the y-axis. Transmittance, T, is the ratio of radiant power transmitted by the sample (I_0) to the radiant power incident on the sample (I0). Absorbance (A) is the logarithm to the base 10 of the reciprocal of the transmittance (T).

$$A = \log_{10}\left(\frac{1}{T}\right) = - \log_{10} T = - \log_{10}(I/I_0) \quad (17)$$

The transmittance spectra provide better contrast between intensities of strong and weak bands because transmittance ranges from 0 to 100% T whereas absorbance ranges from infinity to zero [Shernan, M. 2014].

5. FT-IR spectrometer

FT-IR is the preferred method of infrared spectroscopy. The resulting spectrum after IR passes through the sample represents the molecular absorption and transmission creating a molecular fingerprint of the sample [Thermo Nicolet.2001]. FT-IR spectrometer basically depends on a simple optical device called an interferometer. As shown in the figure below, the interferometer requires two mirrors, an infrared light source, an infrared detector and a beam splitter.
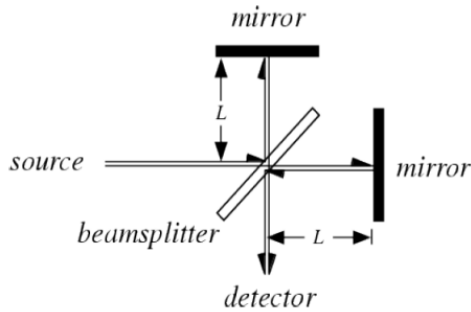
Figure 2.14: The Michelson interferometer (scienceworld.wolfram.com).

The beam-splitter is the heart of the interferometer. Essentially a half-silvered mirror, the beam-splitter reflects about half of an incident light beam while simultaneously transmitting the remaining half. One half of this split light beam travels to the interferometer's moving mirror while the other half travels to the interferometer's stationary mirror. The two mirrors reflect both beams back to the beam-splitter where each of the two beams is again half reflected and half transmitted.

Two output beams result: one travels to the detector as the other travels to the source. When the two beams return to the beam-splitter, an interference pattern, or interfero-gram, is generated. This interference pattern varies with displacement of the moving mirror, with the difference in path length in the two arms of the interferometer. The interference pattern, detected by the infrared detector as variations in the infrared energy level, is what ultimately yields, spectral information [Hsieh, H. N. 2008].

The interferogram is Fourier transformed with the help of computer to convert the space domain into wave number domain [Vij, D. R.2006]. The basic integral equation used in FT-IR spectroscopy can be obtained from the definition of Fourier integral theorem. The basic equation used in the case of Michelson interferometer can be derived as follows: Let the amplitude of the wave (travelling in the z-direction) incident on the beam splitter be given as

$$E(z,v) \, dv = E_0(v) \, e^{i(\omega t - 2\pi vz)} \, dv$$

(18)

Where E_o (v) is the maximum amplitude of the beam at z=0. The amplitude of the beam is divided at the beam splitter and two beams are produced. Let z_1 and z_2 be the distances travelled by the beams when they recombine. Each beam undergoes one reflection from the beam splitter and one transmission through the beam splitter. If *r* and *t* are the reflection and transmission coefficients, respectively, of the beam splitter, then the amplitude of the recombined wave ER is

$$E_R [z_1,z_2,v] \, dv = rt \, E_0 (v) \, [\, e^{i(\omega t - 2_\pi vz1)} + e^{i(\omega t - 2_\pi vz2)}] \, dv$$ (19)

By definition, the intensity after recombination of the beams for the fixed spectral range dv is given as

$$I(z_1, z_2, v) \, dv = E_R (z_1, z_2, v) \, E_R^{\ *}(z_1, z_2, v) \, dv$$

$$= 2 \, E_0^2 (v) \, |rt|^2 \, [1 + \cos 2(z_1 - z_2) \, v] \, dv$$ (20)

And the total intensity at any path difference x=(z1-z2) for the whole spectral range is obtained by integrating equation (24) as

$$I_R (x) = 2 |rt|^2 \int_0^\infty E_0^2(v) \, dv + 2 |rt|^2 \int_0^\infty E_0^2(v) \cos (2\pi xv) dv$$ (21)

Fourier cosine transform of equation (25) converts intensity into spectrum as

$$E_0^2(v) = (\, 1/ \, \pi|rt|^2) \int_0^\infty [I_R (x) - \frac{1}{2} I_R (0)] \cos(2\pi vx) \, dx$$ (22)

In the above equation, I_R (0) represents the flux associated with waves at zero arm displacement where the waves for all frequencies interact coherently. Thus, I_R (0) is the flux associated with coherent interference and IR(x) is the flux associated at path difference x. [I_R (x) − 1/2 I_R(0)] is called the interferogram. The spectrum *S(v),* which is proportional to E_0^2(v) can be given from equation (26) as

$$S(v) \ \alpha \ E_0^2(v) = \text{constant} \int_0^\infty [I_R (x) - \frac{1}{2} I_R (0)] \cos(2\pi vx) \, dx$$ (23)

The interferogram is Fourier transformed with the help of computer to convert the space domain into the wave number domain [Cooper, A. 2004].

For FT-IR measurements, A bruker IFS 66/S spectrometer which is shown in (Fig.2.15.a) was used in the mid-infrared spectral range of (400-40)cm^{-1}.This spectrometer consists of several different modules, which are described in (Table 2.1).The interferometer which is represented in (Fig.2.15.b) is a Michelson interferometer which was described previously in (sec.2.8.2.1) with a KBr beam splitter. And the aperture which was used in 8mm; since we found that this aperture gives the best signal to noise ratio. The sample holder with a hole A

as shown in Figure.2.16 the beam must pass through the center of this hole, and the holder is aligned on a base plate.The spectrometer is continuously purged with dry air during the measurements, where a MCT detector was cooled using liquid nitrogen.
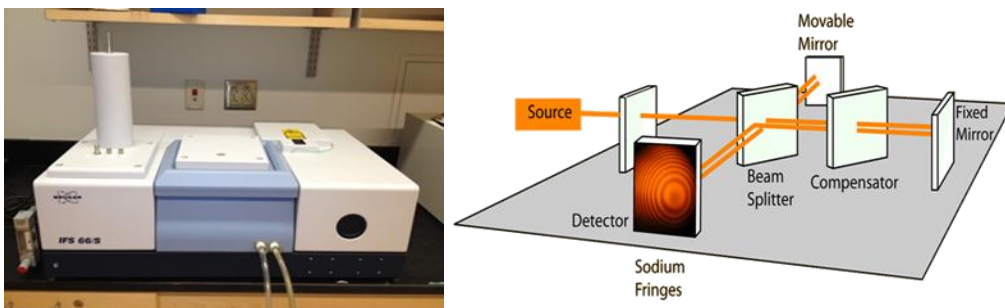
Figure 2.15: (a): Bruker IFS 66/S spectrometer, (b): Michelson interferometer [OPUS Bruker 2004].

Table 2.3: Bruker IFS 66/S spectrometer models and their descriptions [OPUS Bruker 2004].

Module	Contents/ Description
Optical Bench	Interferometer, optics, detector, sample, chamber, vacuum valves.
Electronics unit	Control electronics (source, optics, etc.) power supplies.
Source cooling system	Thermostatically controlled closed loop water circulator for sources.
External vacuum system	Pump, demister, bellows and pipes and valves to pump and backfill the optical bench.
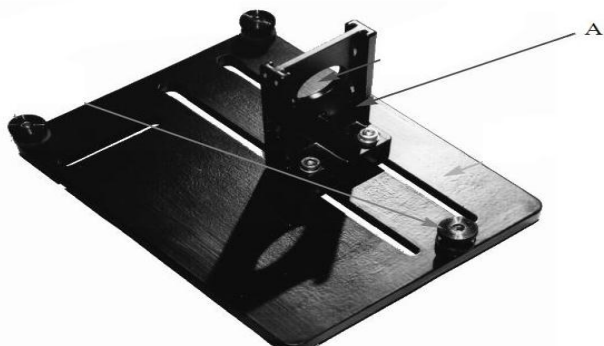
Figure 2.16: The sample holder and its base plate [OPUS Bruker 2004].

Table 2.4: Some of the optional detectors that can be used [OPUS Bruker 2004]

Optional Detector	Operating Temperature
Si diode	Room
Ge diode	Room
InSb	Liquid N_2
FIR- DLATGS	Liquid N_2
MCT	Liquid N_2
InGaAs	Room

6. Sample analysis by FT-IR spectrometer

The normal instrumental process is as follows:

The Source: Infrared energy is emitted from a glowing black-body source. This beam passes through an aperture which controls the amount of energy delivered to the sample (and, ultimately, to the detector).

The Interferometer: The beam enters the interferometer where the "spectral encoding" takes place. The resulting interferogram signal then exits the interferometer.

The Sample: The beam enters the sample compartment where it is transmitted through or reflected off of the surface of the sample, depending on the type of analysis being accomplished. This Is where specific frequencies of energy, which are uniquely characteristic of the sample, are absorbed.

The Detector: The beam finally passes to the detector for final measurement. The detectors used are specially designed to measure the special interferogram signal.

The Computer: The measured signal is digitized and sent to the computer where the Fourier transformation takes place. The final infrared spectrum is then presented to the user for interpretation and any further manipulation [Thermo Nicolet. 2001].
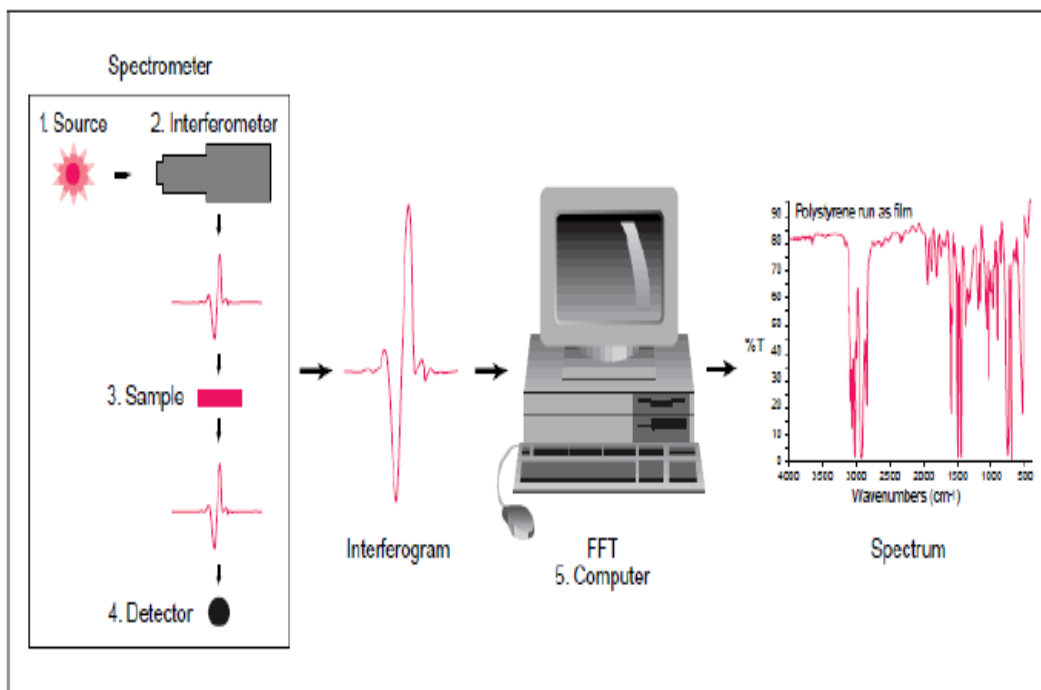
Figure 2.17: FT-IR spectrometer layout and basic components (chemwiki.ucdavis.edu)

2.3 Protein structure

This section is about proteins structures and the domains in ASA to which ligands bind [Griffiths, P.R 2007]

2.3.1 Amino Acids

Amino acids are the building blocks of proteins. a central carbon atom, called the α carbon, linked to an amino group, a carboxy acid group, a hydrogen atom, and a distinctive *R* group. *R* group is referred to as the side chain see figure 2.20 [Smith, A. 2005]. Proteins in living organisms are made from 20 amino acids that are Essentially [Zhang, G. 2008].
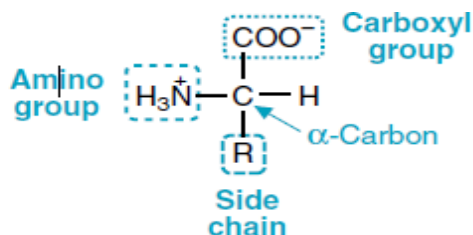
Figure 2.18: General structure of the amino acids found in proteins.

2.3.2 Peptide

Peptide is short chains of amino acids with less than fifty amino acid residues. A common classification for peptides uses the number of amino acid building block in the chain. That is, each building block in the protein chain is called an amino acid residue, whereas a chain of amino acids is called a Peptide.

The word residue comes from the act of residing, after an amino acid forms a peptide linkage upon joining a peptide chain. For instance, a peptide is a short chain with two amino acid residues, a dipeptide are formed by three residues and so forth. Since the terminology becomes burdensome after 12 residues, the peptide chains with more than 12 and less than about 20 amino acid sequences are referred to as oligopeptides. According to this terminology, only when the chain exceeds 20 amino acids in length, the term polypeptide is then used [Berg 2001];[Grisham, G. 1995].

The Peptide Bond

Peptides and proteins are sequential and unbranched polymers of amino acids linked head to tail. In every instance, a carboxyl group of one amino acid is linked to amino group of another amino acid through a type of covalent amide linkage referred to as peptide bonds. When a peptide bond is formed, the reaction releases water molecules Figure 2.19. The peptide "backbone" of a protein follows a repeated sequence –N-Cα-C-, where the N represents the amide nitrogen, the Cα is the α-carbon atom of an amino acid in the polymer chain, and C is the carboxyl group of another amino acid. [Grisham, G. 1995], [Smith, A.2005].
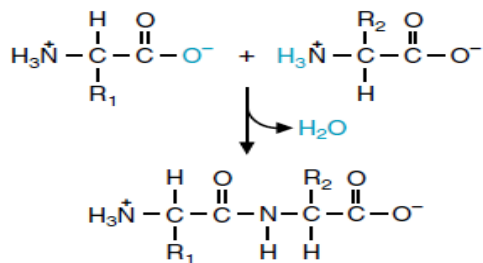
Figure 2.19: Peptide bond. Amino acids in apolypeptide chain are joined through peptide bonds between the carboxyl group of one amino acid and the amino group of next amino acid in the peptide.

Proteins

Proteins have many functions in the body. Structural proteins are the major function in our body, they serve as transporters of hydrophobic compounds in the blood, as cell adhesion molecules that attach cells to each other and to the extracellular matrix, as hormones that carry signals from one group of cells to another, as ion channels through lipid membranes, and as enzymes that increase the rate of biochemical reactions [Smith, A. 2005].

2.3.3 Levels of Protein Structure

To cope with the complex architecture of protein molecules, they have been classified in several levels depending on their structural conformation. Figure 2.20 shows four different levels [Smith, A. 2005].
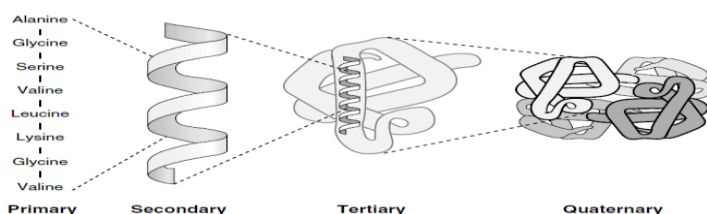
Figure 2.20: Levels structure of proteins.

A.Primary Structure

The amino acid sequence is the primary structure of a protein. A schematic of this conformation is shown in Figure 2.21 [Grisham, G. 1995]. The most proteins in primary structure is not biological functional.
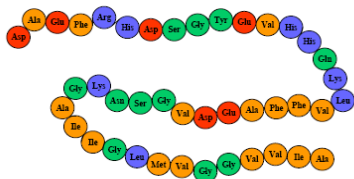
Figure 2.21: Peptide Visualized as a Simple Amino Acid Sequence.

B. Secondary Structure

Regions within polypeptide chains form recurring, localized structures known as secondary structures. The two regular secondary structures called the α-helix and the β-sheet contain

repeating elements formed by hydrogen bonding between atoms of the peptide bonds. Other regions of the polypeptide chain form non regular non repetitive [Grisham, G. 1995].

B.1 The α -Helix

The α-helix is a common secondary structural element of globular proteins, membrane-spanning domains. It has a stable rigid conformation that maximizes hydrogen bonding while staying within the allowed rotation angles of the polypeptide backbone. The peptide backbone of the α-helix is formed by strong hydrogen bonds between each carbonyl oxygen atom and the amide hydrogen (N-H) of an amino acid residue located four residues further down the chain (Figure 2.22a).

Thus, each peptide bond is connected by hydrogen bonds to the peptide bond four amino acid residues ahead of it and four amino acid residues behind it in the amino acid sequence. The core of the helix is tightly packed, thereby maximizing association energies between atoms. The *trans*side chains of the amino acids project backward and outward from the helix, thereby avoiding strict hindrance with the polypeptide backbone and with each other (Figure 2.22b) [Smith, A. 2005].
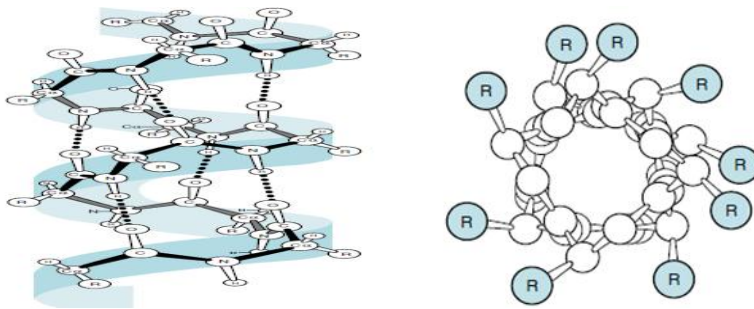
Figure 2.22 a: The α-helix. Each oxygen of a carbonyl group of a peptide bond forms a hydrogen bond with the hydrogen atom attached to a nitrogen atom in a peptide bond four amino acids further along the chain.
b): A view down the axis of an α-helix. The side chains (R) jut out from the b.2 ß -Sheets

ß-Sheets are a second type of regular secondary structure that maximizes hydrogen bonding between the peptide backbones while maintaining the allowed torsion angles. Hydrogen bond networks that hold ß-strands are different in parallel and ant parallel sheets. The parallel ß-sheets have evenly spaced hydrogen bonds that angle across between the ß-strands, whereas ant parallel ß-sheets have parallel narrowly spaced hydrogen bonds that alternate with widely-space pairs Figure 2.23 [Tsai, C. 2007].

Thus, the carbonyl oxygen of one peptide bond is hydrogen-bonded to the nitrogen of a peptide bond on an adjacent strand. (This pattern contrasts with the ß-helix in which the peptide backbone hydrogen bonds are within the same strand.) Optimal hydrogen bonding

occurs when the sheet is bent (pleated) to form **ß**-pleated sheets [Smith, A. 2005], [Serdyuk, I.N. 2007].

A higher level of structure is generated when polypeptide chains assume a more compact three-dimensional shape by bending and folding. For instance, tertiary structure allows proteins to adopt a globular. Tertiary structures are usually seen in those proteins commonly existing in cells. The globular conformation promotes a lower surface-to -volume ratio and shields the protein from interacting with the solvent [Grisham, G. 1995].

D. Quaternary Structure
Many proteins consist of two or more tertiary structures. Each of these tertiary structures is commonly referred to as a subunit of a protein. This subunit organization in proteins constitutes yet another level in the hierarchy of protein structure [Grisham, G.1995].

C. Tertiary Structure
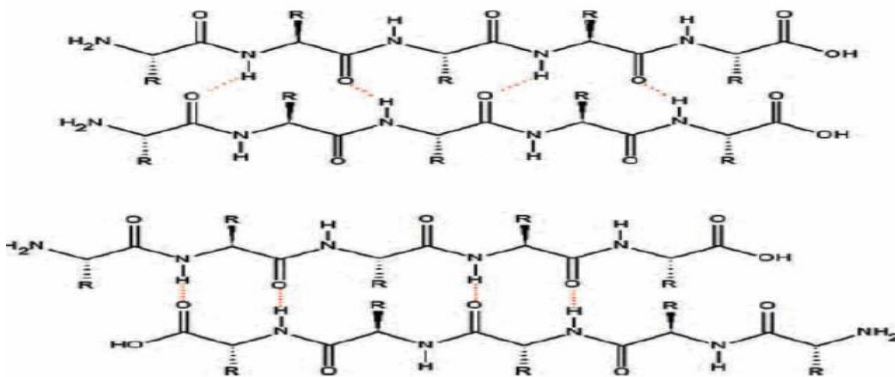
Figure Error! No text of specified style in document.**.23: Parallel (top) and ant parallel (bottom) _ß_sheets**

2.4 BSA Interaction with Gold Particles
In this section we review the BSA interactions with gold nano particles

2.4.1 Bovine Serum Albumin (BSA)
Bovine Serum Albumin (BSA) is a high purity, lyophilized "Fraction V" powder derived from the plasma of USDA-inspected healthy animals located in the USA. Bovine Serum albumin (Figure 2.24) is isolated from other plasma protein products and lipids by a unique proprietary, non-solvent procedure. The purification process includes a modified Cohn/heat-shock procedure designed to inactivate proteases and other potentially interfering enzymes.

Further processing such as extensive membrane dialysis and filtration, minimizes analytes that can cause background interference in sensitive assays as well as inhibition in sensitive cell and microbial culture systems. [Hirayama K. 1990].Bovine Serum Albumin is applicable for numerous biochemical applications including ELISAs (Enzyme-Linked Immunosorbent

Assay), immunoblots, and immunohistochemistry. Frequently used as a blocking reagent; particularly useful with casein-sensitive antibodies, such as phospho-specific antibodies.
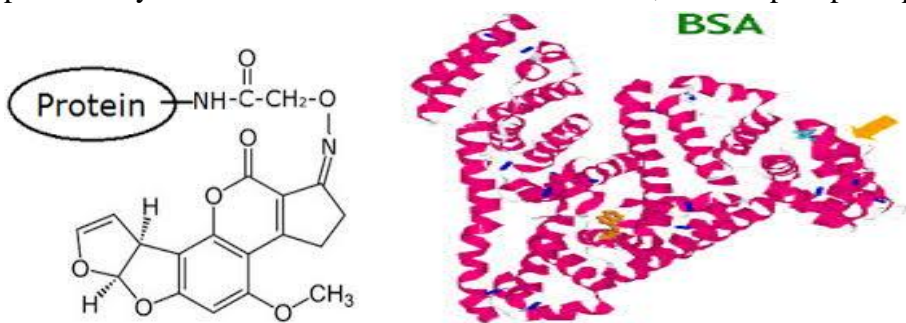
Figure 2.24 : Chemical structure of Bovine Serum Albumin (BSA).

Also used as a nutrient in cell and microbial culture. In restriction digests, BSA is used to stabilize some enzymes during digestion of DNA and to prevent adhesion of the enzyme to reaction tubes and other vessels. Commonly used to determine the quantity of other proteins, by comparing an unknown quantity of protein to known amounts of BSA [Wise SA, 2010].Either Applications are Protease-sensitive Immunoassays such as RIA, EIA, Fluorescent and Chemiluminescent Protein Standard, Diluent Protein, Conjugate or Enzyme Stabilizer Hybridization Selected Cell Culture applications.

2.4.2 Gold Nanoparticles

Properties of gold nanoparticles are different from its bulk form because bulk gold is yellow solid and it is inert in nature while gold nanoparticles are wine red solution and are reported to be anti-oxidant. Inter particle interactions and assembly of gold nanoparticles networks play key role in the determination of properties of these nanoparticles . Gold nanoparticles exhibit various sizes ranging from 1 nm to 8 μm and they also exhibit different shapes such as spherical, sub-octahedral, octahedral, decahedral, icosahedral multiple twined, multiple twined, irregular shape, tetrahedral, Nano triangles, Nano prisms, hexagonal platelets and Nano rods [Deb S 2011], [AK Khan 2014].
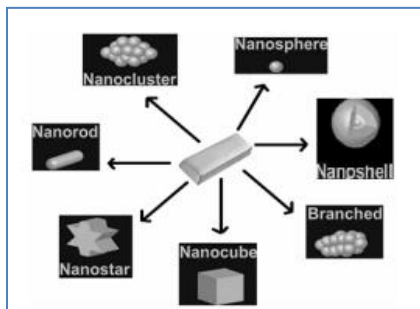
Figure Error! No text of specified style in document.**.25: shapes of gold nanoparticles**

Among all these shapes (Figure 2.25) triangular shaped nanoparticles show attractive optical properties as compared to the spherical shaped nanoparticles. Using of single active substance from plant extract in the synthesis of gold nanoparticles is an important bio synthesis technique to purify gold nanoparticles and to investigate about their medical uses. Gold nanoparticles have been widely used in the field of radiation medicine as radiation enhancer and also provide therapeutic enhancement in radiation therapy due to the efficient and targeted drug delivery to the tumor site.

Gold nanoparticles have various applications as platform nanomaterials for biomolecular ultrasensitive detection, killing cancer cells by hyperthermal treatment, labeling for cells and proteins and delivering therapeutic agents within cells. Fluorescent nanoparticles or nanoprobes based on gold nanoparticles have good biocompatibility for molecular imaging of many enzymes and metabolites which is necessary for cellular functions in cancer. Gold Nano rods have gained much attention in recently few past years due to their specific optical and chemical property and hence used for biological applications [AK Khan, et al.2014].

Gold nanorods have unique anisotropic geometry which enables them to get tunable absorption in both visible and near infrared (NIR) regions and make them suitable for potential applications in the fields of bio-sensing, gene delivery and photo thermal therapy. Gold nanoparticles have various advantages over conventional iodine-based agents as gold has higher absorption coefficient than iodine due to its higher atomic number and electron density so it enhance CT contrast more than iodine so they have been used in X-ray CT imaging as molecular probes .

 The second major advantage of gold nanoparticles is that they are non-cytotoxic and third most important benefit is regarding their surfaces, as they have large surface area due to which their surfaces are readily available for modification with targeting molecules or specific biomarkers and applicable in biomedical purposes.

The role of gold nanoparticles in biological sciences is very important because of the compatibility, conjugation of these particles to the biomolecules and their tunable optical properties which are due to the shape, size and surface area of the gold nanoparticles. Due to the small size and large surface, shape and crystallinity, nanoparticles are proved to be excellent therapeutic agents because they can easily travel into the target cells and can bear high drug load [AK Khan 2014].

Gold nanoparticles are widely used in biomedical science including tissue or tumor imaging, drug delivery, photo thermal therapy and immune-chromatographic identification of pathogens in clinical specimens due to the surface Plasmon resonance (SPR).

Nanoparticles have unique physiochemical properties including surface area, amphilicity, shape, biocompatibilities and surface carrier capabilities which make them suitable for gene delivery, as the function of conjugated gold nanoparticles described by various factors such as protein structure, particle morphology and conjugated strategy. Gold Nano rods have various applications in the field of in vivo imaging due to the plasmons resonance absorption and scattering of light in the near infrared region. Colloidal gold nanoparticles have also gain much attention due to their easy preparation through chemical methods and they can easily be imported to the tissues and cells because of their very small size which is equal to the biological molecules like DNA and proteins

Gold nanoparticles can bind with a wide range of organic molecules as they have low toxicity and tunable physical and chemical properties so they have been used as therapeutic agents or vaccine carriers in to the specific cells so that they can increase the efficiency of drugs and can destroy pathogens. By using gene gun gold nanoparticles have been extensively used for epidermal delivery of DNA vaccines and this method is one of the best methods to deliver DNA vaccine. Coated walls of gold Nano cages with temperature-sensitive polymer were used as drug carrier which releases their effectors with interaction of near-infrared irradiations.
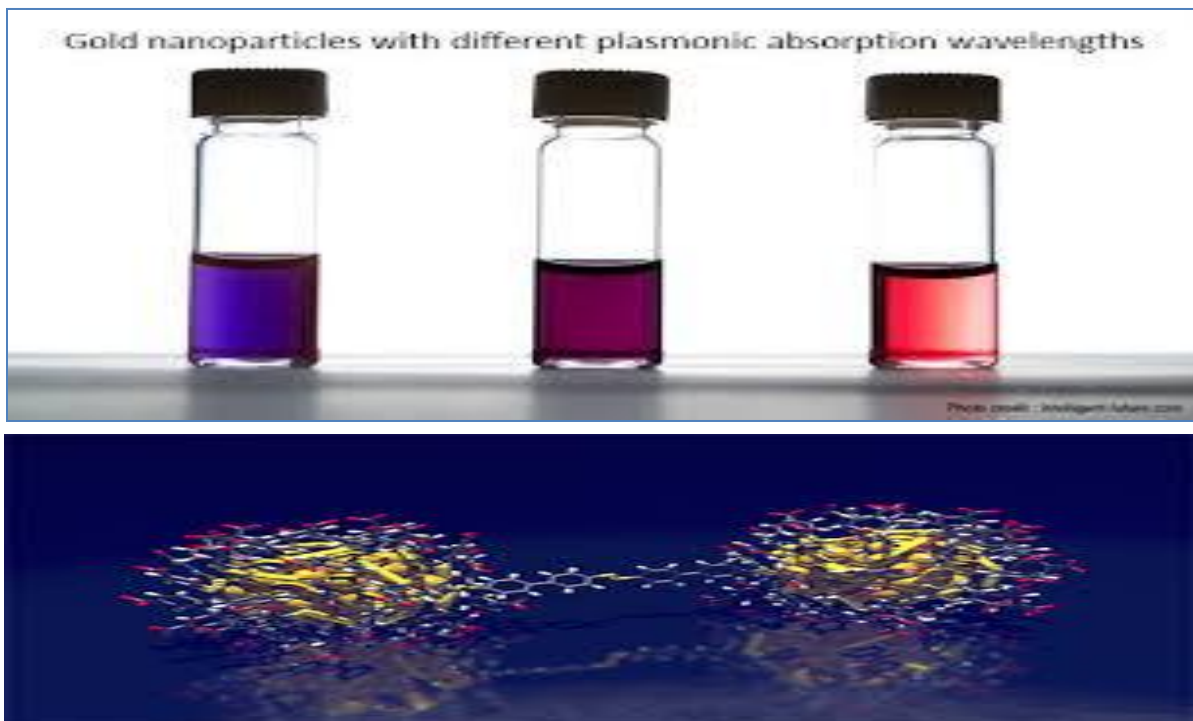
Figure 2.26 : gold nanoparticles with different plasmonic absorption wavelengths.

Gold nanoparticles having small size and diameter about 1 nm are able to cross the cell membrane and nucleus to interact with DNA on the contrary gold nanoparticles of size 18 nm exhibit excellent penetration in to cells but cytotoxicity was not observed . Gold nanoparticles have strong affinity for alkynes as compared to other transition metal catalysts but the homogeneous systems are not favorable economically and environmentally because of rapid reduction of active gold complexes in to inert metallic gold during the C-H alkyne activation.

Due to the unique optical and electronic properties of gold nanoparticles they have been widely used in the color (Figure 2.26) indicating probes in the development of analytical techniques which are used for the sensing of various analytes.

Gold colloids have been used in the surface modification of ideal electrodes due to their remarkable stability and unique properties including high biocompatibility which is necessary to retain the native structure and enzymatic activity of attached proteins or enzymes. Combination of gold nanoparticles into smart polymer like poly (N-isopropylacrylamine) is an effective process to enhance the various properties of polymer such as showing swell of collapse reversibility in response to the temperature stimuli.

Chapter Three: Experiments

3.1 Preparation of Samples

Fatty acid free BSA, and gold nanoparticles in powder form were purchased from Sigma Aldrich chemical company[Hirayama K. 1990] and used without further purifications. The data were collected using samples in liquid form for UV-VIS and Fluorescence measurements and in thin films for FT-IR measurements. Preparation of the thin film samples required several stock solutions as described below.

3.1.1 BSA stock solution

BSA was dissolved in phosphate buffer saline, at physiological pH 7.4, with a concentration of **80 mg/ml**, to get a final concentration of **40 mg/ml** for the BSA-Gold complexes.

3.1.2 Gold nanoparticles stock solution

Gold nanoparticles (**288.42 g/mol**)were dissolved in phosphate buffer saline at (**0.7622 mg/ml**)and room temperature. The solution was placed on a shaker for one hour in order to dissolve the gold powder with phosphate saline, then it was placed in ultrasonic water path (SIBATA AU-3T) for 8 hours to ensure the gold completely dissolved. The solution was placed in a water path with a temperature range 37-40c° for one hour to achieve a homogenous solution.

3.1.3 BSA-Gold nanoparticles complex solutions

The concentrations of the BSA-Gold samples were prepared from mixing the BSA and the Gold according to the 5 ratios (1:1, 1:2, 1:3, 1:4 and 1:5 volume to volume).

Liquid Sample for UV-VIS and FS

A 10 µl sample of gold was pipetted into the end of a fiber optic cable (the receiving fiber). A second fiber optic cable (the source fiber) was brought into contact with the liquid sample causing the liquid to fill the gap between the two fiber optic ends. The gap was controlled to both 1mm and 0.2 mm paths. A pulsed xenon flash lamp provided the light source and a spectrophotometer utilizing a linear CCD array was used to analyze the light after passing through the sample. The process is controlled by PC based software, and the data was logged in an active file on the PC, to determine the binding constant (K).

Before conducting samples measurements, the NanoDrop 1000 spectrophotometer was calibrated or blanked. The spectrum of a reference material (blank) was first stored in instrument memory as an array of light intensities by wavelength. The actual measurement involves recording the intensity of the transmitted light through the sample. The absorbance is calculated according to the following formula for the range of wavelengths

Absorbance = - log (Intensity sample/Intensity blank) (24)

The Beer-Lambert equation is used to correlate the absorbance with concentration.

3.1.4 Thin film for FTIR

NICODOM Ltd silicon windows were used as spectroscopic cell windows. The optical transmission is high with little or no distortion of the transmitted signal. The 100% line of a NICODOM silicon window shows that the silicon bands in the mid-IR region do not exhibit total absorption and can be easily subtracted. 20 µl of each sample of BSA-Gold was spread on the silicon windows and an incubator was used to evaporate the solvent, to obtain transparent thin films on the silicon windows. All solutions were prepared at the same time at room temperature.

3.2 Instruments and procedures

3.2.1 Ultra Violet Visible Absorption Spectroscopy (UV-VIS)

The NanoDrop ND-1000spectrophotometer
The NanoDrop ND-1000 spectrophotometer was used to measure the samples absorption spectra in the range wavelengths range 220-750 nm, with high accuracy and reproducibility. We outline the UV-VIS procedure according to the instructions outlined inNanoDrop1000 V3.7, 2008, User's Manual. The steps are:

1. With the sampling arm open, pipette the sample onto the lower measurement pedestal see photo no.1 of Figure 3.1

2. Close the sampling arm and initiate a spectral measurement using the operating software on the PC. The sample column is automatically drawn between the upper and lower measurement pedestals and the spectral measurement made see photo no.2 of Figure 3.1.

3. When the measurement is complete, open the sampling arm and wipe the sample from both the upper and lower pedestals using a soft laboratory wipe. Simple wiping prevents sample carryover in successive measurements for samples varying in concentrations (Figure 3.1.photo no.3).
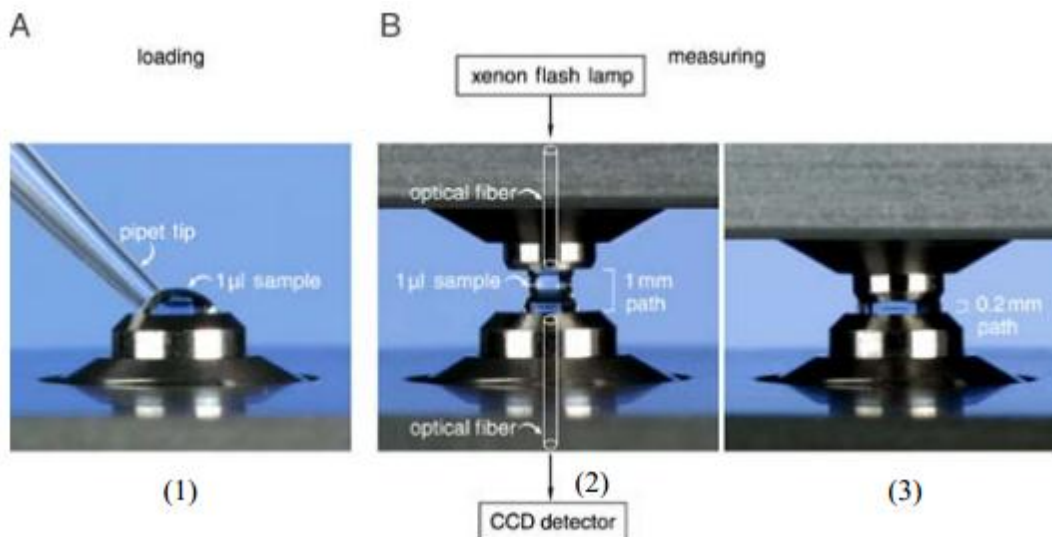
Figure 3.1: UV-VIS procedure steps using the samples with the NanoDrop 1000Spectrophotometer.

3.2.2Fluorospectrometer (NanoDrop 3300)

Fluorescence measurements were performed using the NanoDrop ND-3300 Fluorospectrometer at 25°C. The excitation source comes from one of three solid-state light emitting diodes (LED's). The excitation source options include: UV LED with maximum excitation 365 nm, Blue LED with excitation 470 nm, and white LED from 500 to 650nm excitation. A 2048-element CCD array detector covering 40-750 nm, is connected by an optical fiber to the optical measurement surface. The excitation is done at the wavelength of 360 nm and the maximum emission wavelength is at 439 nm. Other equipment as Digital balance, pH meter, Vortex, Plate stir, and micropipettes were used following the NanoDrop 3300 V2.7 user's Manual 2008 instructions as follows.

1. Before taking measurements on samples the NanoDrop 3300 was blanked.

2. A 10μl sample of gold is pipetted onto the end of the lower measurement pedestal (the receiving fiber).

3. A non-reflective bushing attached to the arm is then brought into contact with the liquid sample to bridge the gap between the arm and the receiving fiber. The gap, or path-length, is controlled to 1mm.

4. Following excitation with one of the three LEDs; the emitted light from the sample passing through the receiving fiber is captured by the spectrophotometer. The NanoDrop 3300 is controlled by software run from a PC.

5. All data is logged and archived in a folder at a user defined location.
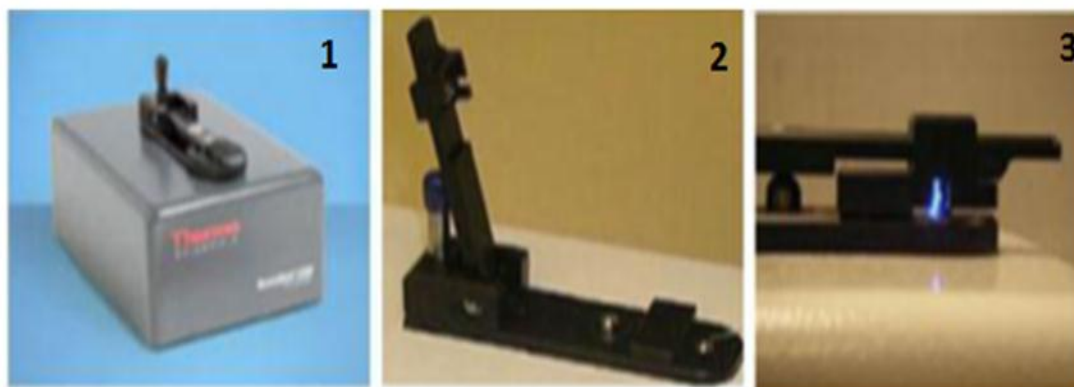
Figure 3.2: Main steps for using the sample with the NanoDrop 3300 Fluorospectrometer.

Basic Use: The main steps for making a measurement are listed below:

1. With the sampling arm open, pipette the sample into the lower measurement pedestal (Figure 3.2 photo no.1).

2. Close the sampling arm and initiate a measurement using the operating software on the PC. The sample column is automatically drawn between the upper bushing and the lower measurement pedestal and the measurement is made (Figure 3.2 photo no.2).

3. When the measurement is complete, open the sampling arm and wipe the sample from both the upper bushing and the lower the pedestal using low lint laboratory wipe (Figure 3.2 photo no.3).

3.2.3 FT-IR Spectrometer
The FT-IR measurements were obtained using a Bruker IFS 66/S spectrophotometer equipped with a liquid nitrogen-cooled MCT detector and a KBr beam splitter. The spectrometer was continuously purged with dry air during measurements.

The absorption spectra were covered the range 400-4000 cm^{-1}. A spectrum comprises an average of 60 scans to improve signal to noise ratio, and the spectral resolution was 4 cm^{-1}. The aperture used was 8 mm, because it gives the best signal to noise ratio. Baseline correction, normalization and peak areas calculations were performed for all the spectra by OPUS software. The peak positions were determined using the second derivative of the spectra. The BSA-Gold complexes spectra, covered the range 1000-1800 cm^{-1}. The FTIR spectrum for free BSA was acquired by subtracting the absorption spectrum of the buffer solution from the protein (BSA) solution spectrum. For the net interaction effect, the difference spectra (BSA. Gold - BSA) spectra were generated using the featureless region BSA solution range of 1800-2200 cm^{-1} as an internal standard [Surewicz, W.K. 1993].

3.2.4 FT-IR data

The analysis of IR spectra to study structure is not straightforward and presents serious conceptual and practical challenge, despite the well-recognized conformational sensitivity of the IR-active bonds. Bands in amide I, amide II and amide III regions are broad, not resolved into individual components corresponding to secondary structure elements. Resolution enhancement or band-narrowing methods are applied to resolve broad overlapped bands into separate bands. FTIR spectroscopy presents several advantages over conventional dispersive methods for this type of analysis through the application of second derivative, peak picking, spectral subtraction, baseline correction, smoothing, integration, curve fitting and Fourier self-deconvolution. In the present study we used the following methods:

1. Baseline correction

The method applied here includes two steps. The first is to recognize the baseline by selecting a point from some spectral points then adding or subtracting intensity from the a point or points to correct the baseline offset. We used this method to bring the minimum point to zero. OPUS successfully removes most baseline offsets [Griffiths P.R 2007],[OPUS Bruker 2004].

2. Peak selection

Automated peak selection involves two steps: the recognition of peaks, and the determination of the wave-numbers for the maximum or minimum absorbance. A threshold absorbance value is usually set to eliminate weak bands [Griffiths P.R 2007].

3. Second derivative

Increased separation of the overlapping bands can be achieved by calculating the second derivative rate of change of the absorption spectrum slope. The method have been successfully applied in a qualitative study for a large number of proteins [Haris P. I. 1999].

4. Fourier self-deconvolution

The Fourier deconvolution procedure, sometimes referred to as 'resolution enhancement' is the most widely used bands narrowing technique in IR for biological materials [Jackson, M. 1981]. Both second-derivative and deconvolution procedures have been applied in a past qualitative study [Workman, J. R. 1998]. In addition to providing valuable information about their secondary structure, the method was useful for detecting conformational changes arising from a ligand binding, pH, temperature, organic solvents, detergents… etc.. In many cases results obtained using this approach were later supported by studies using other techniques such as X-ray diffraction and NMR. However, both derivative and deconvolution techniques should be applied with care since they amplify the noise significantly [Haris, P. I. 1999].

5. Spectral subtraction

Difference spectroscopy is another approach that is very useful for investigating subtle differences in proteins structure. It involves the subtraction of a protein absorbance of state A from that of state B for the same protein. The resultant difference spectrum only shows peaks that are associated with the groups involved in the conformational change [Haris, P. I. 1999]. The accuracy of this subtraction method is tested using several control samples with the same protein or drug concentrations, which resulted into a flat base line formation.

6. Curve Fitting

The Curve Fit command allows calculating single components in a system of overlapping bands. A model consisting of an estimated number of bands and a baseline should be generated before the fitting calculation is started. The model can be set up interactively on the display and is optimized during the calibration.

Chapter Four: Results and Discussion

This chapter includes the main results, and analysis of our data. In the first section, UV-VIS results are discussed. The next section deals with Fluorescence results. In the final section, FTIR data analysis is given. Table 4.1 shows the samples prepared for the various conducted tests with the various concentrations and mix ratios. The samples were prepared from the same original gold or BSA solutions with the concentrations as outlined in the table.

4.1 UV-VIS binding constants for BSA-Gold complexes

The absorption spectra for the various samples (40 and 60 nm) are shown in Figures 4.1and 4.2.The excitation was at 210 nm and the absorption was recorded at 280 nm. The UV absorbance intensity of BSA increased with the increasing of gold ratio ,In addition, the binding of the gold ratio to BSA resulted in a slight shift of the BSA absorption spectrum. These results clearly indicated that an interaction and some complex formation occurred between BSA and gold ratio separately.

Figure 4.1: UV-absorbance spectra of BSA with different molar ratios of 40nm Gold nanoparticles (a = free BSA, b =1:1,c = 1:2, d= 1:3, e = 1:4 and g = 1:5)
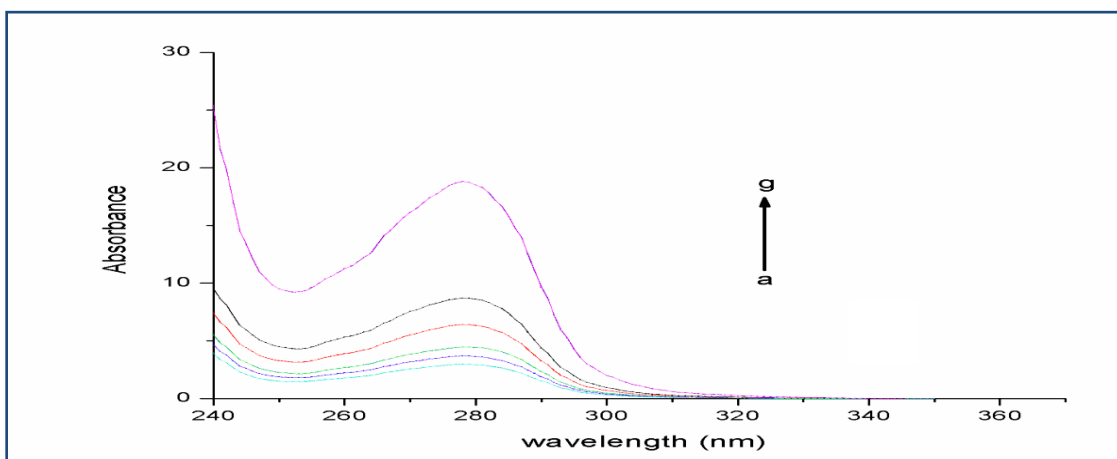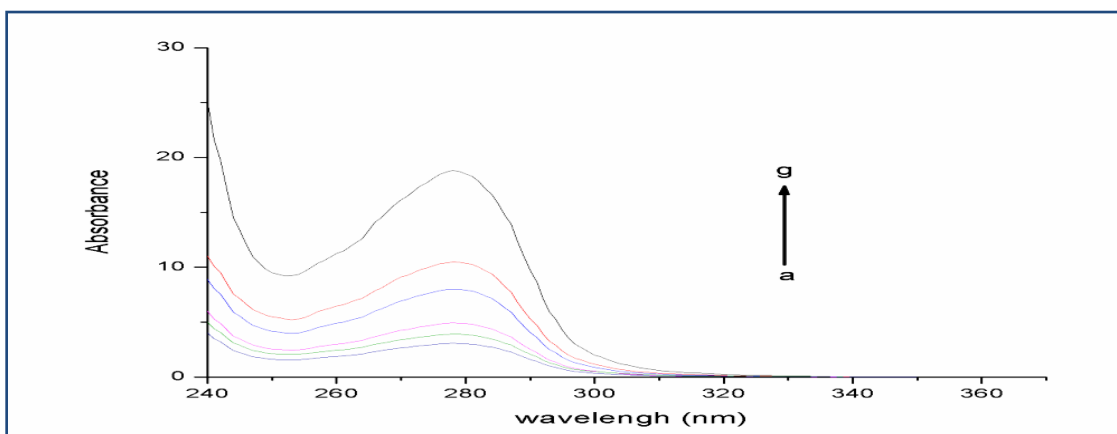

Figure 4.1: UV-absorbance spectra of BSA with different molar ratios of 60nm Gold nanoparticles (a = free BSA, b =1:1, c = 1:2, d = 1:3, e = 1:4 and g = 1:5)

Table 4.1 Samples prepared and used for the various test conducted. Three similar copies of each coded sample were used for the three spectroscopic methods to cover the full range of interest.

- **Solutions prepared at room temperature, concentrations 0.1 mol/l for the BSA and Au 40 & 60nm.**

- **Samples compositions ratios by volume i.e. 1:5 means we prepared 40µlBSA + 40µl gold mixed uniformly then take 40µl for the sample. Gold concentration from the original solution is .76g/l or 2.64 mMol/l; BSA concentration is 40 g/l.**

Code	Composition	Ratios	Spectrometers method and figures	Curves color codes
BSA-1/0	BSA	1:0	UV-VIS 4.1-2 Fluorescence. 4.5-6 FTIR 4.13-14	a_
40-1/1		1:1		b_
40-1/2		1:2	UV-VIS 4.1	c_
40-1/3	BSA:Au40 nm	1:3	Fluorescence. 4.5	d_
40-1/4		1:4	FTIR 4.13	e_
40-1/5		1:5	_	f_
60-1/1		1:1		b_
60-1/2		1:2	UV-VIS 4.2	c_
60-1/3	BSA:Au60 nm	1:3	Fluorescence 4.6	d_
60-1/4		1:4	FTIR 4.14	e_
60-1/5		1:5		f_

4.1.1 Binding constants for BSA-gold nanoparticles complexes using UV-VIS.

BSA-Gold complexes binding constants were determined using UV-VIS spectrophotometer according to published methods [Stephanos, J. 1996], [Koltz 1971], [Ouameur, A. 2004] by assuming only one type of BSA-Gold interaction in aqueous solution, which leads to equation (25-A) and (25-B) as follows:

BSA + Gold ⟷ Gold: BSA   25-a

K = [Gold nanoparticles: BSA] /[free Gold nano particles] [free BSA]   25-b

The absorption data were treated using linear double reciprocal plots based on the following equation [Lakowicz, J. R. 2006]

$$\frac{1}{(A-A_0)} = \frac{1}{(A_\infty - A_0)} + \frac{1}{K(A_\infty - A_0)}\frac{1}{L}$$

(26)

Where A_0 is the initial absorption of protein at 280 nm ; A_∞ is the final absorption , and A is the recorded absorption for the various gold concentrations L. The double reciprocal plot of $1/(A-A_0)$ vs. $1/L$ is linear as shown in Figures 4.3 and 4.4, and the binding constant K was estimated to be $0.888 \times 10^4 M^{-1}$ for BSA-gold (40 nm) complexes and $1.16 \times 10^4 M^{-1}$ for the BSA-gold (60 nm) complexes. The value indicates a weak gold interaction compared to other BSA-drugs complexes with binding constants in the range of $10^5 - 10^6$ M^{-1} [Kargh Hanse, U. 1981].that means the binding constant in gold nano particles 40 nm less than the binding constant in gold nano particles 60 nm.
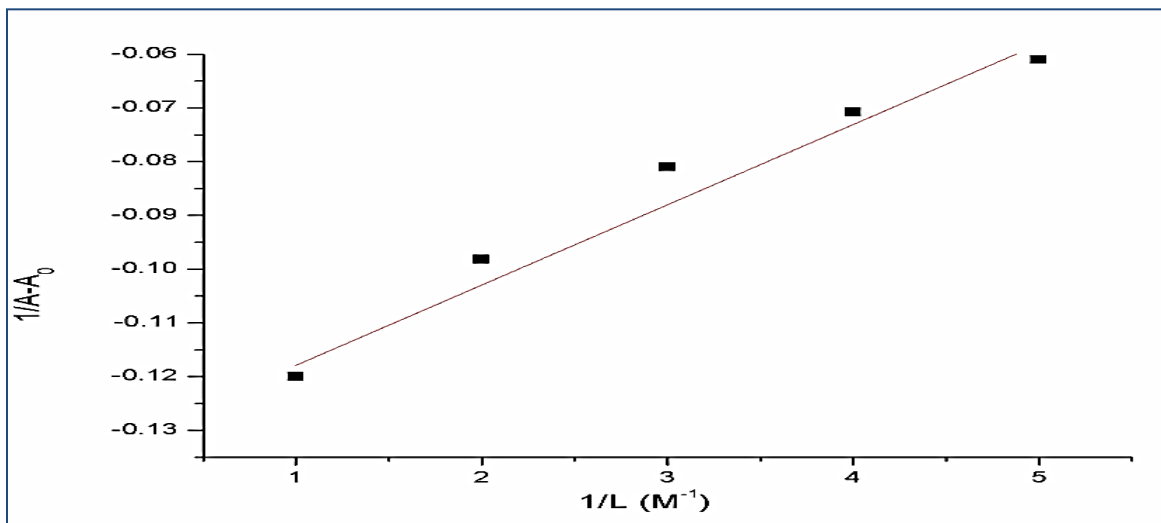
Figure 4.3: $1/(A-A_0)$ vs $1/L$ for BSA with the five BSA: gold 40 nm ratios
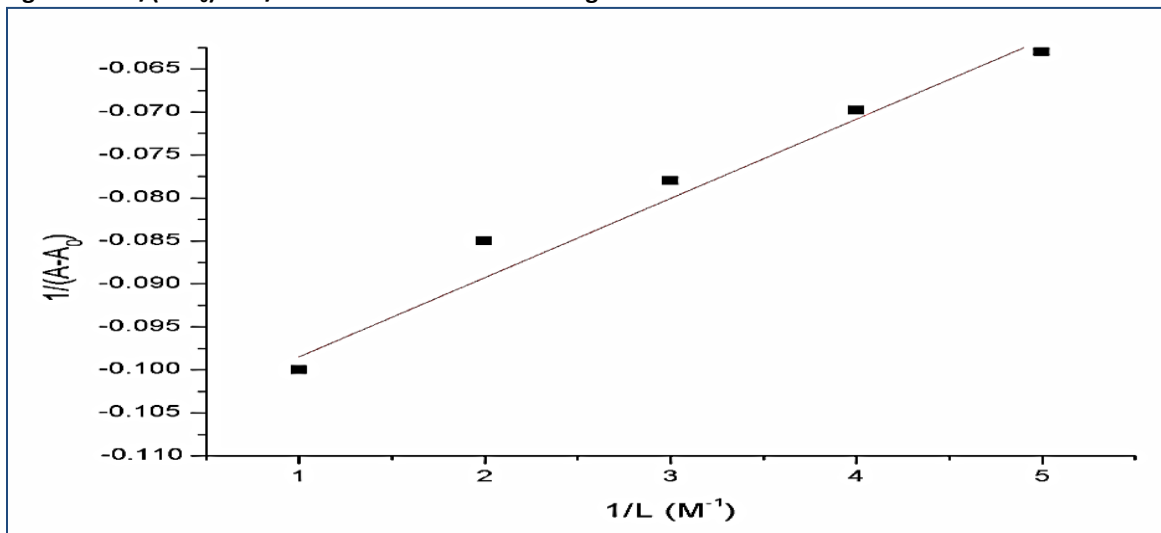
Figure 4.4: $1/(A-A_0)$ vs $1/L$ for BSA with the five BSA: gold 60 nm ratios

4.2 Fluorescence Spectroscopy (FS)

The BSA Fluorescence results are from the tryptophan, tyrosine, and phenylalanine residues. The intrinsic fluorescence of many proteins is contributed mainly from tryptophan, because phenylalanine has very low quantum yield and the fluorescence of tyrosine is almost totally quenched if it is ionized or near an amino group, a carboxyl group, or a tryptophan residue [Darwish, S. M. 2010].

In this work the BSA-Gold excitation wavelength used was 360nm, and the observed wavelength emission was at 439 nm. The fluorescence sensor is based on intramolecular charge transfer (ICT), which is highly sensitive to the polarity of microenvironment. Therefore, it is expected to act as fluorescent probe for some biochemical systems like proteins [Tian, J.N. 2003].
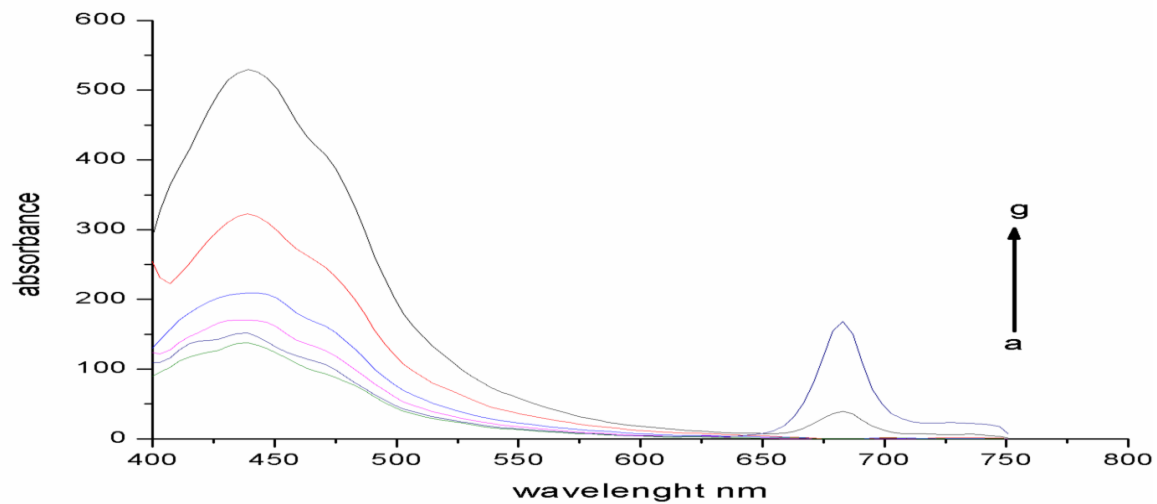
Figure 4.5: Fluorescence emission spectra of BSA with the various BSA-Gold 40 nm ratios (a= free BSA, b =1:1,c = 1:2, d= 1:3, e = 1:4 and g = 1:5).
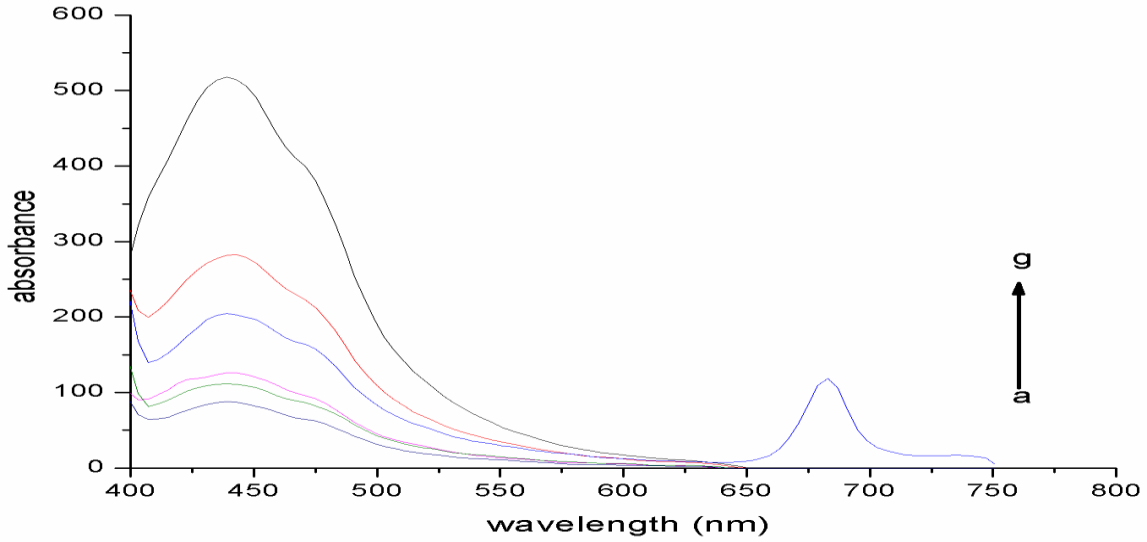
Figure 4.5: Fluorescence emission spectra of BSA with the various BSA-Gold 60 nm ratios (a= free BSA, b =1:1, c = 1:2, d= 1:3, e = 1:4 and g = 1:5).

The BSA fluorescence quenching spectra at various gold ratios (both sizes 40 nm and 60 nm) are shown in Figures 4.5 and 4.6. The BSA fluorescence intensity gradually decreases while the peak position shifts mildly with increasing the gold percentage indicating a BSA-gold interaction. This indicates gold can inhibit or quench the auto fluorescence of BSA, and the BSA-gold interaction modifies the microenvironment around the tryptophan residue with further exposure to the polar solvent as suggested by [Petitpas, I. 2001], [Wang, T. 2008].

4.2.1 Stern-Volmer quenching constants Ksv and the quenching rate constant of the biomolecule Kq

Fluorescence quenching is a bimolecular process that reduces the fluorescence intensity without changing the emission spectrum range. This can be from transient excited-state interactions (collisional quenching) or formations of non-fluorescent ground-state species. Assuming dynamic quenching dominance, the decreased intensity is described by the Stern-Volmer equation:

$$F_0/F = 1+ K_q\tau_0 (L) = 1+ K_{sv}(L) \tag{27}$$

F and F_0 are the fluorescence intensities with and without quencher, K_{sv} is the Stern-Volmer quenching constant, K_q is the bimolecular quenching constant, τ_0 is average lifetime of the biomolecule without quencher, and L is the quencher concentration. K_{sv} indicates the the fluorophore sensitivity to a quencher.

Linear curves based on equation 27 are shown in Figure 4.7 for BSA-Gold complexes. K_{sv} was obtained from the slope of the curves of Figures 4.7 and 4.8, yielding 2.17×10^2 L mol^{-1} for BSA-gold (40nm). From $K_{sv} = K_q \tau_0$, we can calculate K_q using a fluorescence life time of 10^{-8} s for BSA [Cheng, F. Q.2006], yielding a value of 2.17×10^{10} L mol^{-1} s^{-1}.
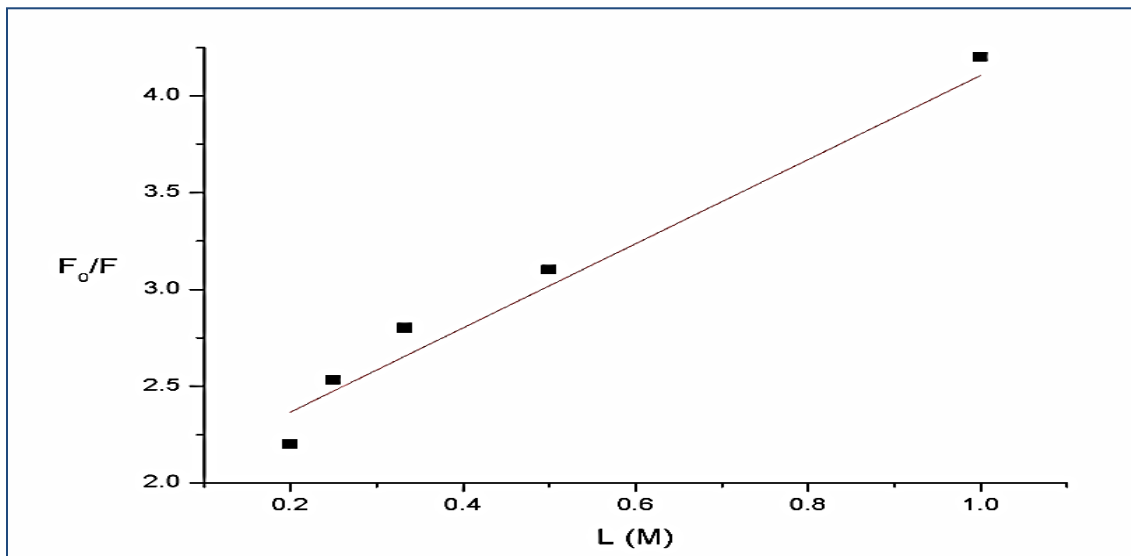
Figure 4.7: The Stern Volmer plot for 40nmGold –BSA complexes.

K_{sv} for BSA-gold nanoparticles (60nm) is 4.5×10^2 L mol^{-1}, and using $K_{sv} = K_q \tau_0$, and fluorescence life time of 10^{-8} s we obtained K_q value of 4.5×10^{10} L mol^{-1} s^{-1}which is larger than the maximum dynamic quenching constant for various quenchers with biopolymer (2×10^{10} L mol^{-1} s^{-1}) [Lakowicz, J. R. 2006]. This implies the quenching is not initiated by dynamic collision but from a complex, static quenching [Wang, T. 2008].
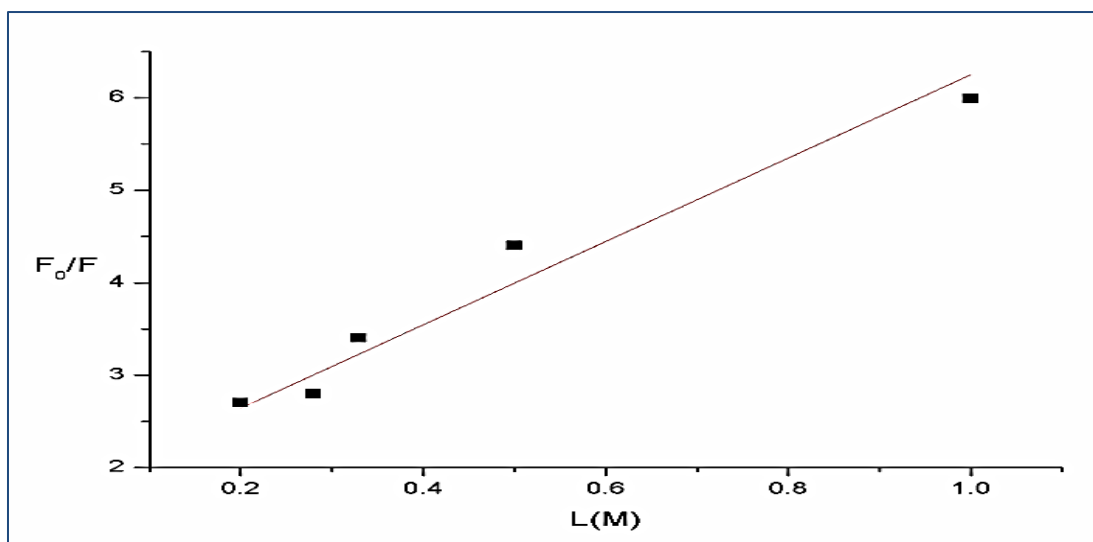
Figure 4.8: The Stern Volmer plot for BSA-Gold 60nm complexes.

4.2.2 Determination of the binding constant

When static quenching is dominant the modified Stern-Volmer equation could be used [Yang, M.M. 1994]

$$\frac{1}{Fo-F} = \frac{1}{FoKL} + \frac{1}{Fo}.$$ (28)

Where K is the binding constant for BSA-Gold, and can be calculated by plotting $1/(F_0-F)$ vs $1/L$, as shown in Figures 4.9 and 4.10.
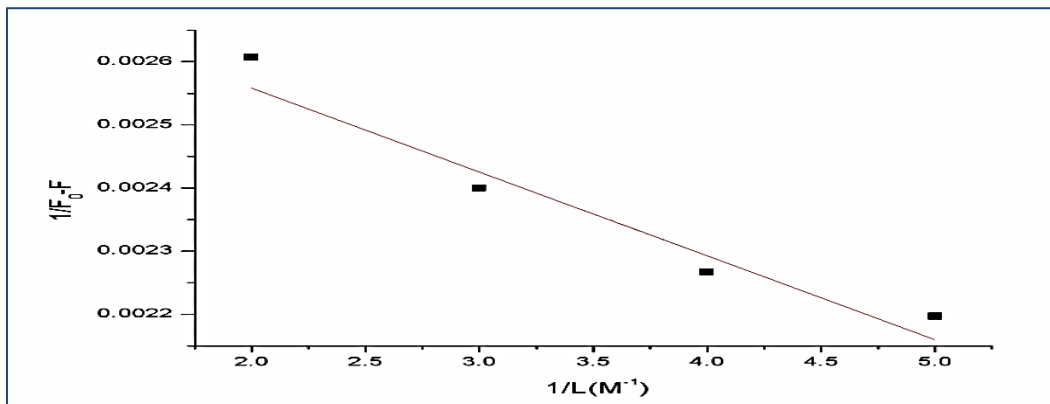
Figure 4.9: The plot of $1/(F_0-F)$ vs $(1/L) \times 10^4$ for BSA Gold40 nm complexes

K equals the ratio of the intercept to the slope. We obtained from Figures 4.9 and 4.10 the K value to be $(0.92 \times 10^4 \text{ M}^{-1}, 1.3 \times 10^4 \text{ M}^{-1})$ and that agrees well with the value obtained earlier from the UV spectroscopy and supports the assumption of static quenching. The highly effective quenching constant in this case has led to a lower value of the binding constant, due to an effective hydrogen bonding between gold and BSA [Darwish, S. M. 2010].

The acting forces between a small molecule and a macromolecule include hydrogen bonds, van der- Waals, electrostatic and hydrophobic interaction forces. In principle both hydrophobic and electrostatic interactions could be involved in the binding process. However, since gold might be largely unionized under the experimental conditions, as expected from its structure, the electrostatic interaction can be excluded.
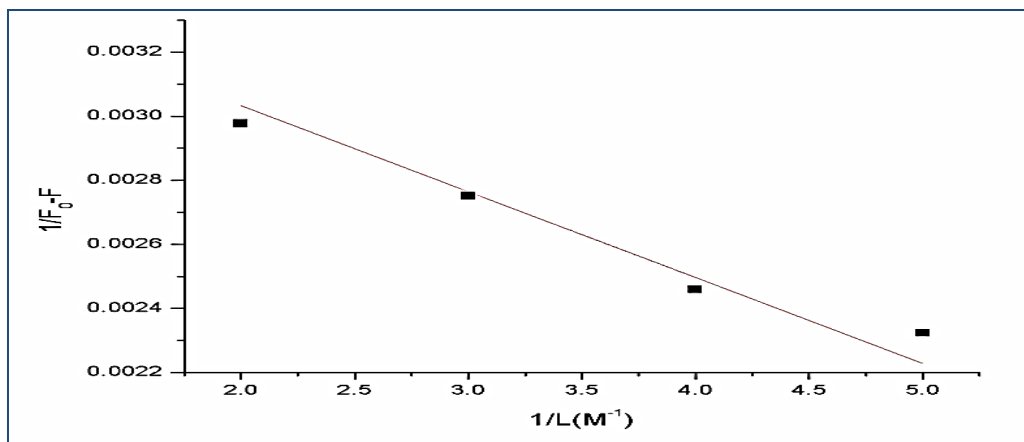
Figure 4.9: The plot of $1/(F_0-F)$ vs $(1/L) \times 10^4$ for BSA Gold60 nm complexes

Thus, gold binding to BSA includes the hydrophobic interaction[Cui, F. 2008], which is mostly an entropic effect originating from the disruption of highly dynamic hydrogen bonds between molecules of liquid water by the nonpolar solutes. Minimizing the number of hydrophobic side chains exposed to water is the principal driving force behind the folding process [Pace C et al. 1996]. Formation of hydrogen bonds within the protein stabilizes the protein structure [Rose G2006].

4.3 FT-IR Spectroscopy

FT-IR transform spectrophotometers have extended the capabilities of infrared spectroscopy and were applied to many areas that are difficult to analyze by dispersive instruments [Shernan, M. 2014]. FTIR spectroscopy provides information about secondary content of proteins. This arises from the amide bands as a result of the groups' vibrations around the peptide proteins bonds [Haris. 1999]. Changing the hydrogen bonds involves peptide linkages occurrence, resulting in changes of the vibrational frequency of the different amide modes of the binding between gold and BSA.
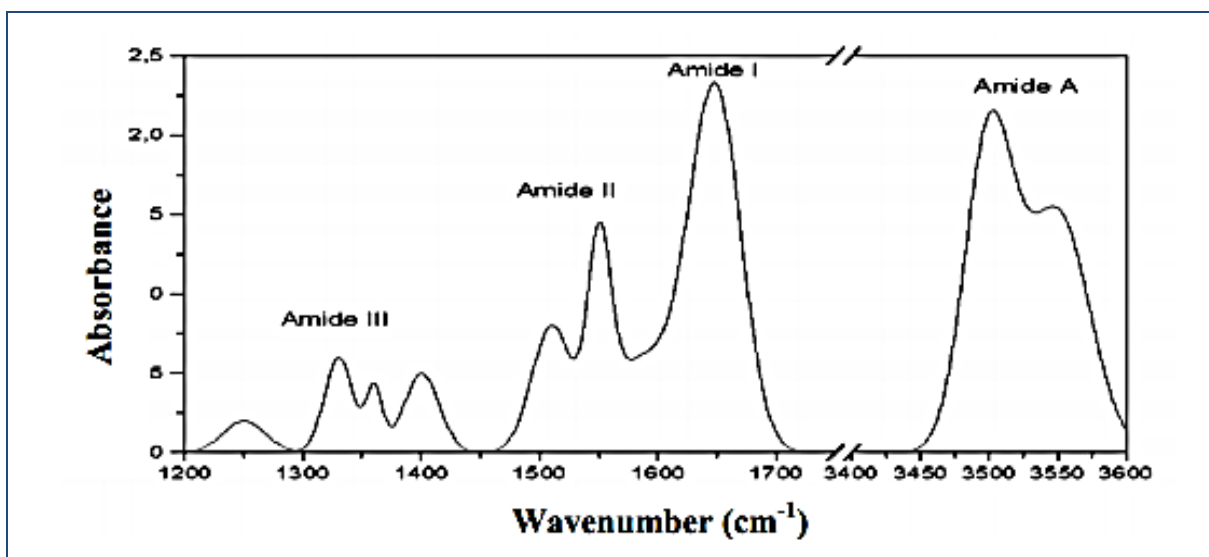
Figure: 4.11: Sample spectrum showing the three relevant regions for determination of protein secondary structure. Amide I (1700-160 cm^{-1}), amide II (160-1480 cm^{-1}), amide III (1330-1220 cm^{-1})

4.3.1. Peak positions

Figure 4.12 shows the second derivative spectra for free BSA, the main absorbance of amide I band was at 1654 cm^{-1} (mainly C=O stretch)and a for amide II band at 1544 cm^{-1} (C-N stretching coupled with N-H bending modes) Figures 4.13 and 4.14show that for all BSA-gold spectra, increasing the gold(both 40nm and 60nm) ratios reduced the amide I, amide II, amide III intensities. The reduction in the is expected to be related to BSA- gold interactions [AbuTair, M 2010].
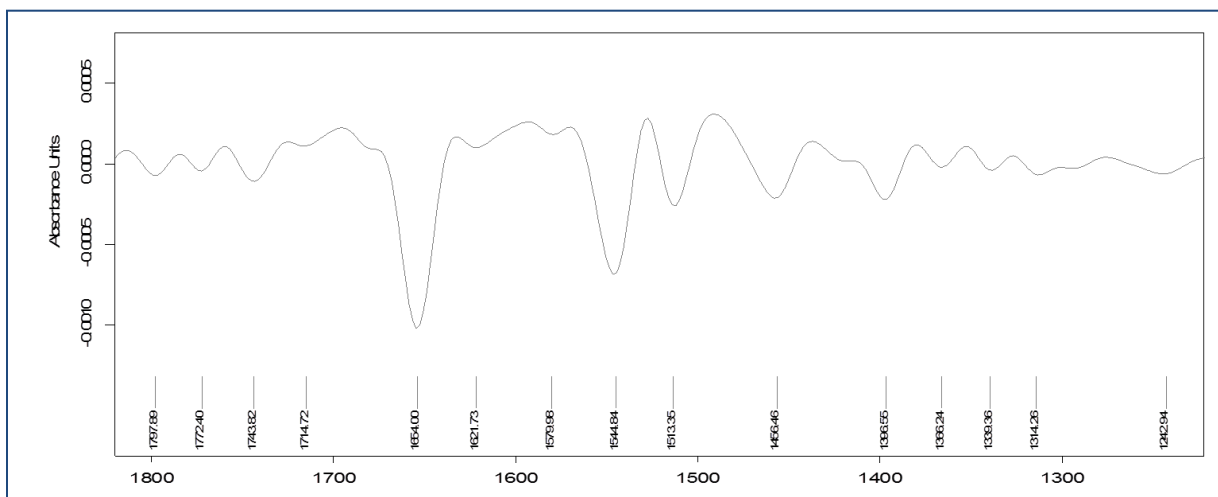
Figure 4.12:   The second derivative of free BSA. The spectra are dominated by absorbance bands of amide I and amide II at peak positions 1656 cm^{-1} and 1545cm^{-1}respectively

Table 4.2 shows the BSA peaks positions the various gold 40 nm ratios. For amide I band the peak positions shifted from 1621 to 1629 cm^{1}, and from 1654 to 1658 cm^{-1}. In amide II they shifted from 1513 to 1523 cm^{-1} and 1579 to 1583 cm^{-1} and new peaks shifted from 1548to

43

1569. In amide III the peaks shifted from 1242 to 1241 cm^{-1}, and from 1314 to 1315 cm^{-1} while the other two peaks shifted down from 1339 to 1335 cm^{-1} and from 1366 to 1361cm^{-1}.
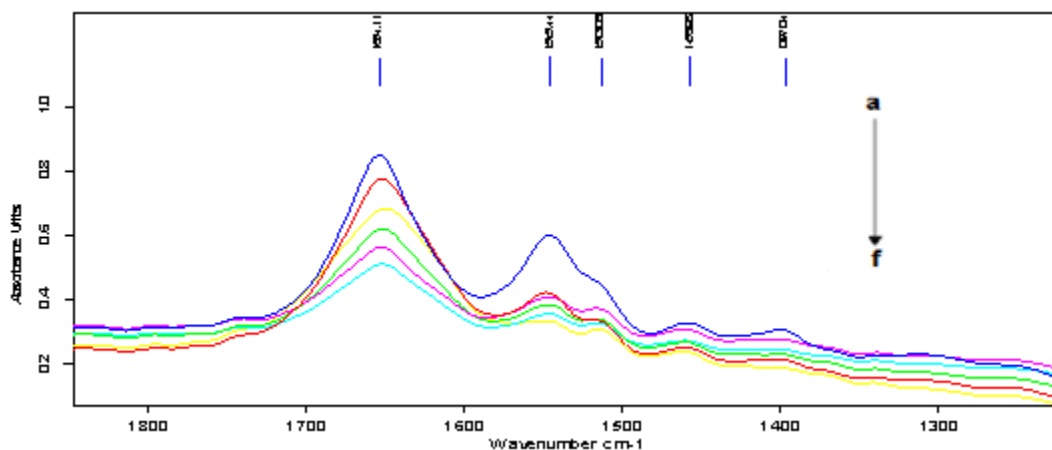
Figure 4.13: Spectra for the various BSA-Gold 40nm ratios. The color codes are outlined in Table 4.1.
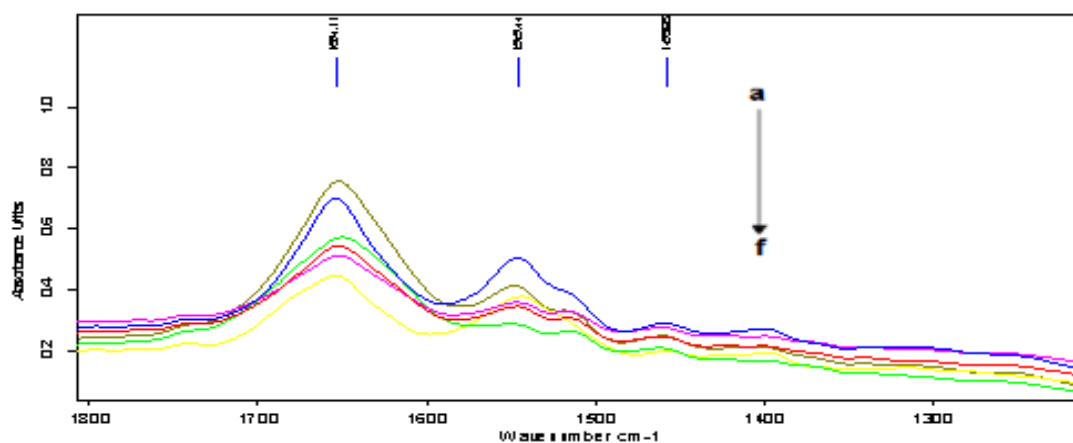
Figure 4.13: Spectra for the various BSA-Gold 60nm ratios. The color codes are outlined in Table 4.1.

Shifts and the change of peaks shape for certain elements can occur due to change in the bonds. The change in peaks shape of BSA for the various gold ratios reflect changes in BSA secondary structure. The shifts are attributed to the newly imposed BSA-Gold hydrogen bonding (on both =O and –OH sites) [AbuTair, M 2010], [Sarver, R.W. 1991]. In **amide I** band, the shift for the second peak was (1621-1629 cm^{-1}) and for the major peak was (1654-1658 cm^{-1}). In amide II the highest shift for the main was (1545-1569 cm^{-1}). Amide III peak shift was observed was (1366-1361 cm^{-1}).

Table 4.3 shows the BSA peaks positions for the gold 60 nm ratios. Amide I peak positions shifted as follows: 1621 to 1626 cm-^{1}, 1654 to 1655 cm^{-1}. In amide II the peak positions shifted from 1513 to 1516 cm^{-1} and 1579 to 1581 cm^{-1}. In addition, a middle peak showed at

44

for high gold ratios and shifted significantly from 1545 to 1557. In amide III the peak positions shifted from 1242 to 1241 cm^{-1}. The peak at 1314 did not shift while the other two peaks shifted down from 1339 to 1332 cm^{-1} and 1366 to 1357cm^{-1}.

Table 4.2: Band assignment in the absorbance spectra of BSA with different Gold nanoparticles 40 nm molecular ratios for amide I, amide II, and amide III regions.

Gold/BSA Bands	Free BSA	1:1	1:2	1:3	1:4	1:5
amide I	1621	1622	1622	1628	1629	1629
(1700-160)	1654	1654	1655	1657	1658	1658
	1513	1513	1517	1521	1521	1523
amide II	1545	1548	1552	1559	1563	1569
(160-1480)	1579	1578	1578	1582	1582	1583
	1242	1242	1241	1243	1241	1241
amide III	1314	1314	1341	1314	1316	1315
(1330-1220)	1339	1339	1338	1337	1335	1335
	1366	1365	1364	1364	1362	1361

Table 4.3: Band assignment in the absorbance spectra of BSA with different gold nanoparticles (60 nm) molecular ratios for amide I, amide II, and amide III regions.

Bands	Free BSA	1:1	1:2	1:3	1:4	1:5
amide I	1621	1621	1622	1623	1623	1626
(1700-160)	1654	1654	1655	1655	1655	1655
	1513	1513	1514	1514	1515	1516
amide II	1545	1547	1551	1552	1554	1557
(160-1480)	1579	1578	1578	1579	1581	1581
amide III	1242	1242	1241	1242	1241	1241
(1330-1220)	1314	1314	1314	1314	1314	1314

1339	1339	1338	1337	1335	1332
1366	13654	1361	1360	1359	1357

In amide I the observed characteristic band shifts often allow the assignment of these bands to peptide groups or to specific amino-acid side-chains. An additional point is the shift of the strong water absorbance away from the amide I region (1610–1700 cm^{-1}) which is sensitive to the protein structure. The minor but reproducible shift indicates that a partial unfolding of the protein occurs in BSA, with the retention of a residual native-like structure. In most cases the peaks shifted toward to high wave numbers. This implies that the of the bond strength increased albeit slightly[Uversky, V.N. 2007].

Chapter Five: Conclusions and Future Work

The interaction between Bovine Serum Albumin (BSA) and gold nanoparticles is interesting and important from pharmaceutical point of view. In this work we have studied the interaction using Ultra Violet Visible Absorption Spectroscopy (UV-VIS), Fluorescence Spectroscopy (FS), and FT-IR spectroscopy for 2 gold nanoparticles sizes of 40 and 60 nm with variable concentrations of BSA as outlined below.

From the UV-VIS spectrophotometer results the binding constants of gold 40nm-BSA are calculated as($0.888 \times 10^4 M^{-1}$), and($1.16 \times 10^4 M^{-1}$) for gold 60nm-BSA complexes. The results indicate a high binding affinity between gold with BAS.

Fluorescence measurements yielded the binding constants values as ($0.92 \times 10^4 M^{-1}$) for gold 40 nm-BSA and $1.3 \times 10^4 M^{-1}$ for gold 60nm-BSA complexes.

FT-IR data indicate that increasing the concentration of both nanoparticles types (40 and 60 nm) lead to BSA unfolding, In addition we may infer that the binding process includes hydrophobic interactions. The newly formed H-bonding results in a C–N bond assuming partial double bond character due to the electrons transfer from C=O to C–N which inhibits the original vibrations. The binding study of nanoparticles (40nm) and (60nm) with BAS .

This research can provide important clinical research information with the theoretical basis for vitamins designs. Further studies are needed to refine the synthesis of nanoparticles as they provide the determinants of the binding site, location, besides thermodynamic parameters like enthalpy free energy and entropy) at variable temperatures to deduce the types of active forces for the binding interactions between gold nanoparticles and BSA.

References

1. [AbuTair, M 2010] Abu Teir, M. M., Ghithan, J. H., Darwish, S. M., Abu-Hadid, M. M. (2010). Journal of Applied Biological Sciences. 4 (3). P79-92.

2. [AK Khan 2014] AK Khan, R Rashid, G Murtaza and a Zahra. (2014). Gold Nanoparticles: Synthesis and Applications in Drug Delivery.p1-p9

3. [Ali, M. E 2012] Ali, M. E.; Hashim, U.; Mustafa, S.; Che Man, Y. B.; Islam, Kh. N. Journal of Nanomaterials 2012, 2012, Article ID 103607.

4. **[**Ball, D.W. 2001] The basics of spectroscopy, SPIE- the international society for optical engineering.

5. [Banwell, C. N.197)] Fundamentals of Molecular Spectroscopy. 2nd ed., McGRAW- HILL Bokk Company (UK) Limited.

6. [Berg 2001] Berg, J. andStryer, L., (2001): Biochemistry, 5th Ed, NewYork.

7. [Cheng, F. Q 2006] Cheng, F. Q., Wang, Y. P., Li, Z.P., Chuan, D. (2006). Spectrochimica Acta Part A, 65, p144.

8. [Cooper, A. 2004] Cooper, A. (2004). Biophysical Chemistry, The Royal Society of Chemistry, UK.

9. [Qui Jiang 2002] C-Qui Jiang M-Xia Gao, and Ji- Xiang He (2002) Study of the interaction between terazosin and serum albumin synchronous fluorescence determination of terazosin. Anal. Chim. Acta. 452, 185-189.

10. [Cui, F. 2008] Cui, F., Wang, J., Li, F., Fan, J., Qu, G., Yao, X., Lei, B. (2008). Chinese Journal of Chemistry, 26, p661.

11. [Darwish, S. M. 2010] Darwish, S. M Abu sharkh, S. E., Abu Teir, M. M., Makharza, S. A., Abu-hadid, M.M.. (2010). Journal of Molecular Structure, 963, p122–129.

12. [Darwish, S.M. 2012] Darwish, S.M. et al. (2012), spectroscopic investigation of pento parbital interaction with Transthyretin, vol 2013, p10, journal of spectroscopy.

13. [Deb S 2011] Deb S, Patra HK, Lahiri P, Dasgupta AK, ChakrabartiK,Chaudhuri U. Multistability in platelets and their response to gold nanoparticles. Nanomed: NanotechnolBiol Med 2011; 7: 376-384.

14. [Derrick. M. R 1999] Derrick, M.R., Stulik, D., Landry, J.M.. (1999): Infrared Spectroscopy in Conservation Science. The Getty Conservation Institue, Los Angelos.

15. **[**Dong, C. Y 2002**]** Dong, C.Y., So, P.T.. (2002). Fluorescence Spectrophotometry. Massachusetts Institute of Technology, macmillan Publishers Ltd.

16. [Dugaiczyk A. 1983] Dugaiczyk A (July 1983). "Linkage of the evolutionarily-related serum albumin and alpha-fetoprotein genes within q11-22 of human chromosome 4". American Journal of Human Genetics. 35 (4): 565–72.

17. [E. K. Oyakawa 2004] E. K. Oyakawa, B. H. Levedahl (2004), Testosterone binding to bovine and human serum albumin: The role of tyrosine groups.

18. [Griffiths, P. R 2007] Griffiths, P. and Haseth, J. (2007): Fourier Transform Infrared Spectrometry. 2nd ed, John Wiley & Sons-Hoboken, New Jersey.

19. [Gordon G. Allison 2011] Gordon G. Allison (2011). Application of Fourier Transform Mid-Infrared Spectroscopy (FT-IR) for Research into Biomass Feed-Stocks, Fourier Transforms - New Analytical Approaches and FT-IR Strategies, Prof. Goran Nikolic (Ed.), ISBN: 978-953-307-232-6.

20. [Grisham, G. 1995] Grisham, G. and R H Garrett (1995) Biochemistry, Saunders College Publishing: Harcourt Brace, Orlando, FL. pp 1154.

21. [Haris1999] Haris, P. I., Severcan, F. (1999). Journal of Molecular Catalysis B: Enzymatic, 7, P 207.

22. [Hawkins JW 1982] Hawkins JW, Dugaiczyk A (1982). "The human serum albumin gene: structure of a unique locus". Gene. 19 (1): 55–8.

23. [Hirayama K. 1990] Hirayama K, Akashi S, Furuya M, Fukuhara K (Dec 1990). "Rapid confirmation and revision of the primary structure of bovine serum albumin by ESIMS and Frit-FAB LC/MS". Biochemical and Biophysical Research Communications. 173 (2): 639–46.

24. [Hollas, M. J. 2004] Hollas, J. (2004): Modern Spectroscopy, 4th, John Wiley & Sons Ltd, UK.

25. [Hsieh, H. N. 2008] Hsieh, H.N. (2008): FT-IR lab instruction, New Jersey Institute of Technology: http://www-ec.njit.edu/~hsieh/ene669/FT-IR.html

26. [Jackson, M.1981] Jackson, M., Mantsch, H.H. (1991). J. Chem., 69, p 1639.

27. [Johnson, L 2010] Johnson. L., Spence. T. Z. M. (2010). Fundamental of fluorescence. Molecular Probes Handbook, A Guide to Fluorescent Probes and Labeling Technologies.11th ed.

28. [Kargh Hanse, U. 1981] Kargh-Hanse, U.(1981) Pharmacol. Rev., 33, p17.

29. [lakowicz, J. R. 2006] Lakowicz, J. R. (2006): Principles of Fluorescence Spectroscopy, 3rded, Springer Science Business Media, LLC .

30. [Maruthamuthu, M. 1987] Maruthamuthu, M., and S. Kishore (1987) Binding of naproxen to bovine serum albumin and tryptophan modified bovine serum albumin. Proc. Ind. Acad. Sci. (Chem. Sci.), 99, 273-279.

31. [Morse, P. M. 1929] Morse, P. M. (1929). "Diatomic molecules according to the wave mechanics. II. Vibrational levels". *Phys. Rev*. 34. pp. 57–64.

32. [NanoDrop 3300 Fluorospectrometer V2.7] user's Manual, 2008, Thermo Fisher Scientific.

33. [NanoDrop 1000 Spectrophotometer V3.7] User's Manual, 2008, Thermo Fisher Scientific.

34. [Nikolić, G. S. 2011] Nikolić, G. S. (2011) Fourier Transforms - New Analytical Approaches and FT-IR Strategies, InTechJanezaTrdine 9, 51000 Rijeka, Croatia.

35. [OPUS Bruker 2004] OPUS Bruker manual version 5.5, 2004 BRUKER OPTIK GmbH.

36. [Ouameur, A. 2004] Ouameur, A., Mangier, S., Diamantoglou, R., Rouillon, R., CarpentierH. A., Tajmir, R. (2004). Effects of Organic and Inorganic Polyamine Cationson the Structure of Human Serum Albumin. Biopolymers, Vol. 73, 503–509.

37. [Pavia 2009] Pavia, D. L., Lampman, G. M., Kriz, G. S., Vyvyan, J. R (2009): Introduction to Spectroscopy, 4th, Brooks/Cole, Cengage learning, USA.

38. [Petitpas, I. 2001] Petitpas, I., Bhattacharya, A. A., Twine, S., East, M., Curry, S. (2001). Journal of Biological Chemistry, 276, P 22804.

39. [Raaman, N. 2006] Raaman, N. (2006). Phytochemical Techniques, New India publishing agency.

40. [Rose G, 2006] Rose G, Fleming P, Banavar J, Maritan A (2006). "A backbone-based theory of protein folding". Proc. Natl. Acad. Sci. U.S.A. 103 (45).

41. [Sathyanarayana, D.M. 1983] Sathyanarayana, D.M. (1983). Vibrational spectroscopy: theory and application. 1st ed,.New age international (P) Ltd., New Delhi.

42. [Schulman, S.G. 1977]Florescence and phosphorescence spectroscopy: physiochemical principles and practice, Vol 59, A. Wheaton & Co. Ltd, Exeter.

43. [Serdyuk, I.N. 2007] Serdyuk, I.N., Zaccai, N.R., Zaccai, J. (2007): Methods in Molecular Biophysics Structure, Dynamics, Function, Cambridge University Press, New York.

44. [Sharma, B.K. 2007] Sharma, B.K. (2007). Spectroscopy. 20ed. Goel Publishing house, Meerut, Delhi.

45. [Shernan, M. 2014] Shernan, M. (2014). Infrared Spectroscopy: A Key to Organic Structure, Yale-New Haven Teachers Institute.

46. [Smith, A. 2005] Smith, A., Marks, M., Colleen, M. (2005): Marks' Basic Medical Biochemistry: A Clinical Approach, 2nd ed, Lippincott Williams & Wilkins.

47. [Smith, B.C. 2011] Smith, B.C. (2011), Fundamentals of Fourier Transform Infrared Spectroscopy, 2nd ed. CRC press, tailor and Francis Group LLC.

48. [Soukpo´e-Kossi2007] Soukpo´e-Kossi, C. N. N., Sedaghat-Herati, R.,C., Hotchandani, S., Tajmir-Riahi, H.A. (2007) International Journal of Biological Macromolecules, 40, p 484–490.

49. [Stephanos, J. 1996] Stephanos, J., Farina, S., Addison, A. 1996. Biochem.Biophys.Acta, 1295.

50. [Stuart, B. 2004] Stuart, B. &John Wiley & Sons, Ltd.(2004), Infrared spectroscopy fundamentals and applications, ANTS, pp. 25–54.

51. [Surewicz, W.K. 1993] Surewicz, W.K., Mantsch, H., Chapman, D. (1993). Biochemistry, P 389.

52. [Thermo Nicolet, 2001] Introduction to Fourier Transform Infrared Spectrometry, Thermo Nicolet Corporation, USA.

53. [Tian, J.N. 2003] Tian , J.N., Liu, J.Q., Zhang, J. Y., Hu, Z.D., Chen, X.G.(2003). Chem.Pharm. Bull., 51, P 702.

54. [Tsai, C. 2007] **Tsai** ,C. Chen MC, Chang Y, Lai WY, Mi FL, Liu CT, Wong HS, Sung HW,(2007),Bio macromolecules: Introduction to Structure, Function, New Jersey, QP801.P64T78

55. [Uversky, V. N. 2007] Uversky, V.N., Permykov, A.E. (2007):Methods in Protein Structure and Stability Analysis; Vibrational spectroscopy, Nova Science Publishers, Inc, Hauppauge, New York.

56. [Vij, D. R.2006] Handbook of Applied Solid State Spectroscopy, Springer Science Business Media, LLC, USA.

57. [Wang, T. 2008] Wang, T., Xiang, B., Wang, Y., Chen, C., Dong, Y., Fang, H., Wang, M. (2008). Colloids Surf. B, 65, P113.

58. [Wilson, E. 1995] methods of experimental physics: spectroscopy, vol 13, A, Academic press Inc.

59. [Wise S. A. 2010] Wise S.A., Watters RL (2010-06-30). "Bovine Serum Albumin (7 % Solution)" (pdf). Certificate of Analysis. United States National Institute of Standards & Technology. Retrieved 2011-12-22.

60. [Workman. J .R. 1998] Applied Spectroscopy: Optical Spectrometers, Academic Press, San Diego.

61. [Yang, M.M 1994] Yang, M.M., Yang, P., Zhang, L.W. (1994). Chin. Sci. Bu, 39, p734.

62. [Zhang, G. 2008] Zhang, G., Que, Q., Pan, J., Guo, J., 2008. J. of Molecular Structure, 881, p132.

الملخص

أشرف جواعدة

إشراف د. موسى أبو طير ـ د. حسين سمامرة

تم دراسة التفاعلات بين جزيئات زلال المصل البقري (BSA) وجسيمات نانو الذهبية (AuNPs) والتغيرات التوافقية ل BSA الناتجة عن هذا التفاعل من خلال مجموعة قياسات التحليل لامتصاص الأشعة فوق البنفسجية والمطياف الضوئي الفلورسنتي وتحويل فورييه للأشعة تحت لنسب مختلفة من جسيمان النانو الذهبية بحجمين 40 و 60 نانومتر مع زلال المصل وتم الإعداد ضمن الظروف المعيارية.

وتم حساب قيم الثابت التفاعلي باستخدام طيف امتصاص الأشعة فوق البنفسجية والمرئية (UV-VIS) عند درجة حرارة الغرفة لمخاليط جسيمات نانو الذهب (40 and 60 nm) مع BSA ليكون ($0.888 \times 10^4 M^{-1}$) و ($1.16 \times 10^4 M^{-1}$) على التوالي، وبحساب التحليل الطيفي fluorescence ا لنفس جسيمات نانو الذهب والظروف كانت قيمة الثابت التفاعلي ($0.92 \times 10^4 M^{-1}$) و ($1.30 \times 10^4 M^{-1}$) لحجمي الذهب على التوالي. بالإضافة إلى ذلك تم حساب ثابت ستيرنفولمر لنفس النماذج وكانت القيمة ($2.17 \times 10^2 L mol^{-1}$) و ($4.5 \times 10^2 L mol^{-1}$) لحجمي الذهب على التوالي.

وكشفت بيانات fluorescence عن انخفاض في كثافة الانبعاثات مع زيادة تركيز جزيئات الذهب نانو. ويشير هذا الانخفاض في الكثافة إلى أن جزيئات الذهب النانوية لديها قدره قويه علي إخماد الفلورة الذاتية لجزيئات BSA من خلال آلية التبريد الساكنة.

تم تعيين مختلف مواقع الذروة لأطياف amide I and amide II and amid III من خلال بيانات فورييه للأشعة تحت الحمراء ودراسة أية تأثيرات ناجمة عن تغيير التركيز لعينات مشابهة وبحجمي الذهب السابقين. وتشير قياسات الأطياف العاكسة إلى حدوث تغير في كثافة نطاقات الامتصاص بسبب تغير الربط مع التركيز. وأظهرت مواقع قمم النطاقات الثلاثة انزياحا نحو اليمين في حين أن آخر قمتين بعد وسط أميد الثالثة كان السلوك معاكسا.

ويستنتج من مجمل بيانات الأطياف ازدياد الربط التفاعلي بين جزيئات الذهب والبروتين مع زيادة حجم جسيمات الذهب كما متوقع. وانقلاب الانزياح للقمم الأخيرة لأميد الثالثة يؤكد تزايد قوة الربط مما كسر الروابط السابقة وتم تكون روابط جديدة. وأظهرت شدة الامتصاص الارتباط والاعتماد على تركيز BSA حيث انخفضت الكثافة عموما مع زيادة تركيز جزيئات الذهب. ورغم أن قوة الترابط بين الذهب والبروتين أقل من كثير من العقاقير الأخرى إلا أن فوائد الذهب وحياديته العامة تجعل استخدامها محبذا رغم النقص.

نقترح مزيدا من التحقق ودراسة تأثير حجم جسيمات الذهب لأحجام مقاربة وتأثير ذلك على التفاعل مع بروتينات أخرى.